research report

Direct Strength Prediction of Purlins with Paired Torsion Bracing

RESEARCH REPORT RP19-3

October 2019

Committee on Specifications
for the Design of Cold-Formed
Steel Structural Members

American Iron and Steel Institute

DISCLAIMER

The material contained herein has been developed by researchers based on their research findings and is for general information only. The information in it should not be used without first securing competent advice with respect to its suitability for any given application. The publication of the information is not intended as a representation or warranty on the part of the American Iron and Steel Institute or of any other person named herein, that the information is suitable for any general or particular use or of freedom from infringement of any patent or patents. Anyone making use of the information assumes all liability arising from such use.

Old Dominion University

Department of Engineering Technology

Direct Strength prediction of purlins with paired torsion bracing

Michael W. Seek
Principal Investigator

Submitted to
American Iron and Steel Institute
Committee on Specifications

ODU Research Foundation
Project # 400327-010

October 4, 2019

Table of Contents

Acknowledgements……..…….…….……..……3
Executive Summary……..…….…….……..……4
Background…….…….…….…….…….…..….5
Methodology Development from Base Tests…..…….…….…..……7
Comparison to Base Tests..…….…….…….……...….16
Diaphragm Stiffness for Strength Evaluation...…….…….……22
Analysis of Purlins in Sloped Roof Systems…….…….……..…24
Predicted Strength of Sloped Roofs…..…….…….…….……..27
Conclusions…….…….…….…….……..30
References…..…….…….…….…….……..32
Appendix 1: Equation Summary for Sloped Roof Systems – Single Span
and Multi-span Interior……..…….……...33

Acknowledgements

The author would like to acknowledge the American Iron and Steel Institute for their support of this project through the Small Project Fellowship Program. This program helps researchers to explore important topics and advance our understanding of the cold-formed steel systems. The author would also like to thank the Metal Building Manufacturers Association for their support of this project. MBMA members shared their expertise, knowledge and time to guide this research project and provide valuable feedback to refine the report. These members of the steering and review committee are recognized below.

Steering and Review Committee

Vincent Sagan, MBMA
Rick Haws, Nucor Building Systems
Jay Larson, American Iron and Steel Institute
Karim Malak, Pinnacle Structures, Inc.
Richard Starks, Building Research Systems, Inc.
Don Tobler, American Buildings Company
Zachary Walker, Behlen Building Systems
Dennis Watson, BC Steel Buildings, Inc.

Executive summary

A methodology to predict the local and distortional buckling strength of purlins with paired torsion bracing using the Direct Strength method has been developed. The procedure is based on the component stiffness method that utilizes a displacement compatibility approach to calculate the anchorage forces in a purlin system. The procedure considers the partial diaphragm restraint provided by the sheathing and incorporates both first order and approximate second order torsion effects to predict the actual distribution of stresses along the cross section of the purlin. This distribution of stresses can vary substantially from the conventionally assumed constrained bending distribution and thus, correspondingly, the predicted local and distortional buckling strength can differ substantially.

To validate the methodology, the procedure has been used to predict the strength of a series of 12 base tests. The test series included 8 in. and 10 in. deep lipped Z-sections with both thin (0.057 in.) and thick (0.100 in.) profiles. The same standing seam deck and clips were used in all of the tests. The detailed investigation into the behavior of the base test revealed several slight load imbalances that, when properly accounted for, can have an impact on the predicted strength. The comparison between the tested strength and predicted strength showed good correlation and the methodology was largely able to predict test anomalies such as failures at the brace location versus the mid-span and failures of the eave purlin versus the ridge purlin. The prediction methodology ignores the additional torsional restraint provided by the sheathing and thus generally resulted in a slightly conservative approximation of the local and distortional buckling strength.

The methodology was expanded to consider slope effects in real roof systems. Equations are provided to predict the strength of simple span and multi-span interior (fixed-fixed end conditions) sloped roof systems. Equations have not been included for multi-span end bays (pinned-fixed end conditions) as the asymmetry requires additional work. As downslope forces are applied to the roof system, they affect the lateral displacement of the diaphragm and thus have an impact on the distribution of stresses along the purlin cross section. A comparison of the changes in stresses is provided. In general, as the slope of the roof increases, lateral deflection of the diaphragm is reduced and the distribution of stresses approaches the constrained bending distribution. There is a corresponding increase in strength. As the slope of the roof gets much steeper, and the lateral deflection of the purlins moves downslope, the predicted strength decreases substantially. In this case of steep roof slopes, it is believed that there is substantial inelastic reserve capacity, that when accounted for will show improved predicted strength.

Background

Paired torsion bracing is commonly used in purlin roof systems supporting standing seam sheathing. Although many configurations are possible, the methodology developed in this report applies to a pair of torsion braces placed symmetrically about the mid-span of the purlin. The braces are considered torsion only, that is, they do not provide lateral restraint to the purlin. One of the advantages of this system, is that since lateral restraint is not provided by the brace, it need not be anchored externally. All of the lateral restraint is provided by the sheathing. To accomplish this torsion only bracing configuration, torsion braces are commonly applied between two adjacent purlins, and only needs to be applied in alternating spaces between the purlins as shown in Figure 1a. The braces are commonly configured either with a channel connected to each purlin or diagonal angles as shown in Figure 1b.

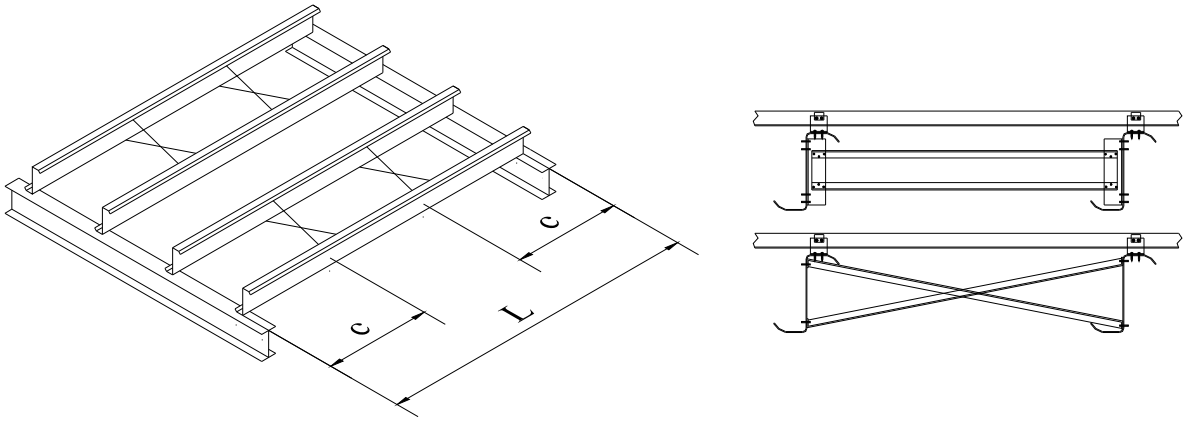

a) bay layout of torsion braces b) common torsion brace configurations

Figure 1. Paired torsion braces

The component stiffness method, which was developed to predict the anchorage forces in purlin systems (Murray et al. 2009), utilizes displacement compatibility to evaluate the forces interacting between a system of purlins, sheathing, and external braces. To develop the strength prediction methodology presented in this report, the component stiffness method is expanded to estimate member geometric second order effects and calculate the actual distribution of stresses in the purlin cross section. By considering the interaction between the purlins, sheathing and braces, biaxial bending and torsion effects are accounted for in the calculation of the true distribution of stresses. This stress distribution can deviate substantially from the typically assumed constrained bending assumption as shown in Figure 2. This drastic change in the distribution of stresses causes two important changes when predicting the strength. First, when considering biaxial bending and torsion, first yield in the cross section will be reached at a lower load level than if the purlin is considered fully constrained. Second, the change in stress distribution has a large impact on the predicted local and distortional buckling strength.

For a low slope roof under gravity loads, as the purlin translates upslope, compressive stresses are reduced at the tip of the top flange and increased at the web flange juncture. The stress gradient in the top flange, shifts the critical location for local and distortional buckling away from the flange tip towards the web-flange juncture. This shift in stresses is consistent with some test results, where local buckling is observed at the web-flange interface. Figure 3 shows the buckling curves for the stress distributions shown in Figures 2 a) and 2 b). For the constrained bending stress distribution, the buckling curve has both a local and distortional buckling minima.

As biaxial bending and torsion are incorporated into the stress distribution, the local buckling minima is decreased and the distortional buckling mode is virtually eliminated.

In a similar manner, the methodology predicts the strength based on the stress distribution at the brace location. Because at the brace location a large concentrated torque is applied to the purlin, there is a spike in the torsion stresses at the brace location. The direction of this concentrated torque depends on the configuration of the system of purlins. In some cases, the torque will resist the tendency of the purlins to roll upslope, whereas in other configurations, the torque resists a downslope roll of the purlins. In either case, the concentrated torque at the brace causes a different stress distribution than at the mid-span location as shown in Figures 2 b) and 2 c). In some cases, the difference in stresses is large enough such that the location of the predicted failure will be away from the mid-span at the brace location. This failure mode away from the mid-span is also consistent with some test results.

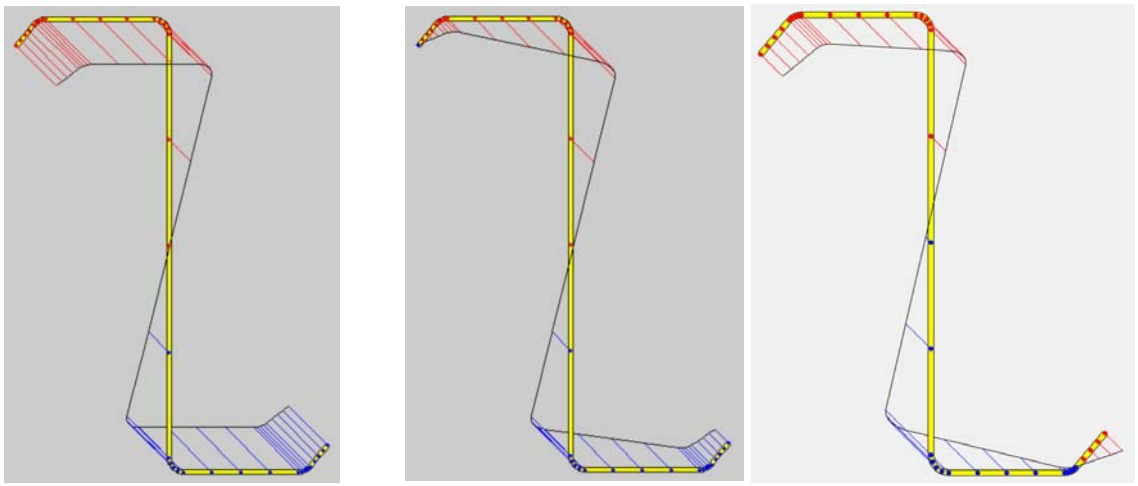

a) constrained bending b) mid-span true stress c) brace location true stress

Figure 2 Comparison of Stress Distribution

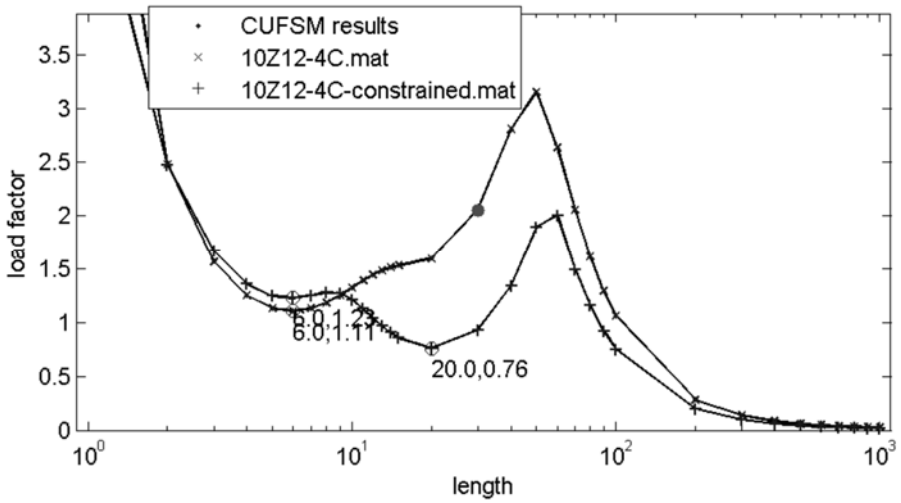

Figure 3. Finite Strip Buckling Analysis constrained bending stress (+) versus true stress (x)

Methodology development from base tests

The methodology was developed and validated based on the results of a series of base tests performed by Emde (2010). The process to apply the procedure to evaluate the base tests is summarized below.

1. Quantify the imbalances of applied load
2. Determine the in-plane force in the diaphragm
3. Determine the torsion effects on purlin
    a. First Order
    b. Second Order
4. Determine the restraining torque provided by the paired torsion braces
5. Determine the additional forces to maintain equilibrium of purlins
6. Determine the cross section normal stresses caused by biaxial bending effects
7. Determine cross section normal stresses caused by torsion effects
8. Perform finite strip analysis to determine local and distortional buckling coefficients
9. Calculate the nominal moment capacity

Although the intent of the analysis procedure is to eventually eliminate the need to perform the base test to determine strength, for those that have existing base test data, applying the procedure to existing data can provide insight into the behavior of these systems. The analysis procedure can be used to refine the diaphragm stiffness for use in design and it can provide a lower bound value for estimating the strength of torsion braces as well as providing a lower bound value for the shear strength of the diaphragm.

Applied load imbalances

The Base Test (AISI 2017c) is a test performed to evaluate the strength of purlin supported standing seam roof systems. The test specimen, as shown in Figure 4, is comprised of two purlins in a simple span configuration spaced at the intended spacing of the roof system (usually five feet) and topped with the roofing panel system that includes all of the insulation components. The specimen is built in a three sided chamber that is sealed on the fourth side with a plastic membrane. A vacuum is drawn within the chamber to simulate applied pressures on the roof system. In a real roof system, purlins are typically installed with the top flanges pointed in the upslope direction. Likewise, in the base test, purlins are installed with the top flanges facing in the same direction towards the "ridge" or the "upslope" side of the chamber. The other side of the chamber is the "eave" or the "downslope" side.

While the base test is a valuable tool to predict the strength of purlin roof systems, care must be taken in interpreting and evaluating the results of the test. There are several subtle imbalances in the base test procedure that must be accounted for. For flexible diaphragms common with standing seam systems, second order effects can be introduced into the test. Including these effects has an impact on the interpretation of the results.

In the base test, the pressure is applied uniformly as the vacuum is drawn in the chamber. The uniformly distributed dead load, u_d, includes the purlin and panel self-weight in addition to the weight of insulation, braces along the span, and the plastic sheathing. The uniform live load, u_p, includes not only the pressure applied to the panel but also the portion of the sheathing that is draped between the end of the panel to the edge of the chamber, the distance, *gap*, as shown in

Figure 4. The balanced uniform load on each purlin, w_{1st} is calculated by

$$w_{1st} = \frac{u_d\,(\text{panel}) + u_p\,(\text{panel} + \text{gap})}{2} \tag{1}$$

The force from the panel is transferred to the purlin flange at an eccentricity relative to the web, e_{sx}, as shown in Figure 4. Because the base test is constructed such that the panels are symmetric relative to the purlin web, effectively there is additional load applied to the eave purlin and corresponding decrease in the load applied to the ridge purlin as shown in Figure 5. This imbalance is accounted for by adding an additional uniform load, w_e, resulting from this eccentricity to the eave purlin and subtracting the same uniform load, w_e, from the ridge purlin. Thus, Figure 5 shows the net force transferred from the sheathing to each purlin flange. The net force transferred to the eave purlin is $w_{1st} + w_e$ whereas the net force transferred to the ridge purlin is $w_{1st} - w_e$. To account for the difference in the direction of forces acting on the eave purlin versus the ridge purlin, the term ξ is used, where $\xi = 1$ for the eave purlin and $\xi = -1$ for the ridge purlin. Note, all analysis presented here was performed based on an eccentricity of 1/3 of the flat width of the flange (i.e. $e_{sx} = 1/3$ b). Some informal parametric studies showed this eccentricity to have the best correlation.

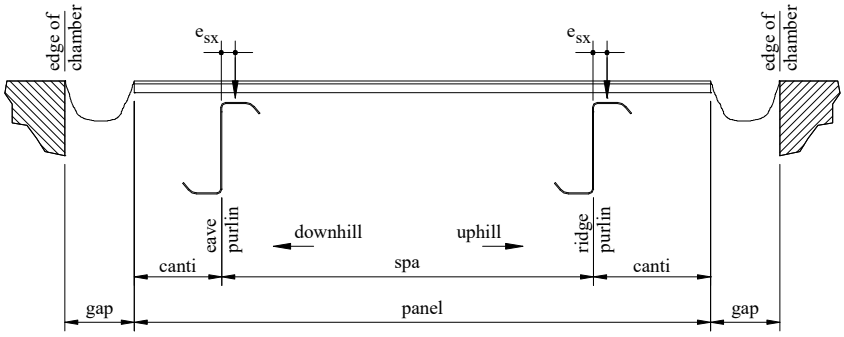

Figure 4. Nomenclature for base test evaluation (Seek and Parva 2018)

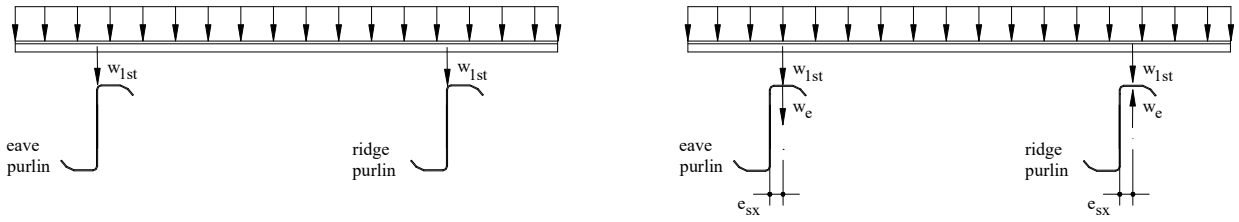

a) without flange eccentricity (b) including flange eccentricity

Figure 5. Panel-purlin transfer of forces (Seek and Parva, 2018)

The additional uniform load resulting from the applied load imbalance is calculated by

$$w_e = w_{1st}\left(\frac{2e_{sx}}{spa}\right)\xi \tag{2}$$

There is also a second order effect that causes additional load imbalance to be shifted towards the eave purlin. As the pressure is increased on the test specimen, as a result of the inclined

principal axes, the system of purlins will deflect laterally at the mid-span by the amount, Δ_{mid}. The gap between the end of the sheathing and the edge of the chamber will increase on the eave side and decrease on the ridge side. As the plastic sheathing sealing the specimen to the chamber transfers force to the edge of the panel, this force will increase on the eave side proportionally to the increase in the gap and decrease on the ridge side correspondingly. These second order forces, w_{2nd}, are added to the eave and subtracted from the ridge. These forces, which have a parabolic distribution with the peak at the mid-span of the purlin, are calculated by

$$w_{2nd} = u_p \left(\frac{\Delta_{mid}}{2}\right)\left(\frac{panel}{spa}\right)\xi \tag{3}$$

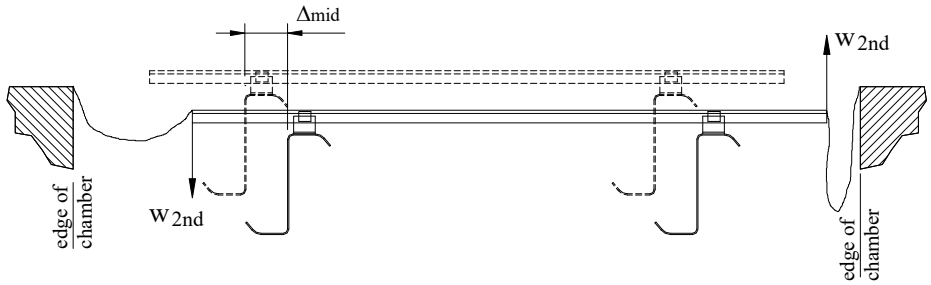

Figure 6: Second order force redistribution (Seek and Parva 2018)

Diaphragm in-plane forces

Displacement compatibility is utilized to determine the in-plane forces interacting between the purlin and the sheathing. Lateral displacement compatibility between the purlin and sheathing is determined at the torsion brace location. This displacement compatibility assumes that the torsion braces are rigid and there is no rotation of the purlin at the brace. For a purlin subject to a uniformly distributed gravity load, the restraining force in the diaphragm along the span of the purlin is uniform. The force in the diaphragm, w_{rest}, is proportional to the applied gravity load, w, by the relationship,

$$w_{rest} = w \cdot \sigma \tag{4}$$

where

$$\sigma = \frac{C_1 \dfrac{\left(\dfrac{I_{xy}}{I_x}\right) L^4}{EI_{my}}}{C_1 \dfrac{L^4}{EI_{my}} + C_2 \dfrac{L^2}{G' \dfrac{panel}{2}}} \tag{5}$$

and

$$C_1 = \frac{1}{24} \cdot \left(\frac{c}{L}\right) \cdot \left[1 - 2\left(\frac{c}{L}\right)^2 + \left(\frac{c}{L}\right)^3\right] \tag{6}$$

$$C_2 = \frac{1}{2} \cdot \left(\frac{c}{L}\right) \cdot \left[1 - \left(\frac{c}{L}\right)\right] \tag{7}$$

where

G′	= stiffness of diaphragm, lb/in.
L	= purlin span
panel	= width of sheathing panel
I_{my}	= modified moment of inertia = $\frac{I_x I_y - I_{xy}^2}{I_x}$
c	= distance from support location to brace location (see Figure 1)

For evaluating the base test, the symbol, σ, is used to represent the proportion of the *gravity* load that translates into an in-plane force in the diaphragm. For sloped roof systems, it is more appropriate to define the in-plane force in the diaphragm relative to the applied force *perpendicular* to the plane of the sheathing. To highlight this subtle distinction, the terminology is changed for sloped roof systems such that the term, ρ, represents the proportion of the force applied perpendicular to the plane of the sheathing that results in an in-plane force in the diaphragm. Additional discussion on this difference is discussed in the section: *Analysis of purlins in sloped roof systems*.

Once the proportion relating the uniformly applied gravity load to the force generated in the diaphragm is determined, the mid-span lateral deflection of the diaphragm, Δ_{mid}, is calculated by

$$\Delta_{mid} = \frac{\sigma \cdot w_{panel} L^2}{8G'(panel)} \tag{8}$$

where, w_{panel} is the total load contributing to the lateral displacement of the diaphragm after the dead loads are in place.

$$w_{panel} = u_p\,(panel + gap) \tag{9}$$

The positive directions for forces and moments as they act on the purlin as well as the positive directions for displacements are shown in Figure 7.

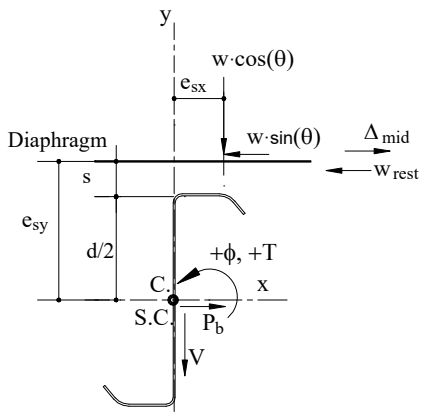

Figure 7 Positive directions for forces and displacements

Torsion

As a point symmetric section, Z-sections are inherently subject to torsion. When tested according to the standard base test, there are additional torsion effects that must be considered. From first order load effects, the purlin is subject to uniform torsion along its length. Forces perpendicular to the plane of the sheathing are applied to the top flange at an eccentricity of, e_{sx}, relative to the shear center of the purlin. Additionally, the uniform lateral restraint provided by the sheathing, w_{rest}, is applied at an eccentricity of e_{sy}, inducing torsion. Note that this eccentricity of the sheathing should incorporate the effective standoff, s, of the purlin as described by Seek and McLaughlin (2017). Considering these two effects, the first order uniform torsion is

$$t_{1st} = \left(w_{1st} + w_e\right)\left(\sigma \cdot e_{sy} - e_{sx}\right) \tag{10}$$

Additional second order torsion effects are caused by the lateral deflection of the purlin. The second order torsion effects are approximated to have a parabolic distribution along the span. For several of the second order torsion effects, the direction of the torque is dependent upon the location of the purlin (eave or ridge).

$$t_{2nd} = -w_{2nd} \cdot e_{sx} - \left(w_{1st} + \left(w_e + w_{2nd}\right)\right)\Delta_{diaph} \tag{11}$$

Restraining torque in torsion braces

The uniform and parabolic torsion are balanced by the torsion braces along the span. The resisting moment by the braces is determined by displacement compatibility between the torsion brace and the purlin. The torsion brace is assumed to be rigid. The concentrated torque that the brace exerts on the purlin as the brace resists the first order uniform torsion is

$$T_{1st} = -C_3 t_{1st} L \tag{12}$$

where

$$C_3 = \frac{1}{4} \cdot \frac{1 - 2\left(\frac{c}{L}\right)^2 + \left(\frac{c}{L}\right)^3}{3\left(\frac{c}{L}\right) - 4\left(\frac{c}{L}\right)^2} \tag{13}$$

The concentrated torque that the brace exerts on the purlin, T_{2nd}, as the brace balances the second order torques with a parabolic distribution, is

$$T_{2nd} = -C_4 t_{2nd} L \tag{14}$$

where

$$C_4 = \frac{1}{15} \cdot \frac{3 - 5\left(\frac{c}{L}\right)^2 + 3\left(\frac{c}{L}\right)^4 - \left(\frac{c}{L}\right)^5}{3\left(\frac{c}{L}\right) - 4\left(\frac{c}{L}\right)^2} \tag{15}$$

Forces to maintain equilibrium of braces

The moment at each end of the brace must be balanced by a shear force at each end as shown in Figure 7. The brace shear force from the first order brace torque, V_{1st}, is

$$V_{1st} = \frac{2C_3 w_{1st} L \left(\sigma \times e_{sy} - e_{sx}\right) \xi}{spa} \tag{16}$$

The brace shear force from the second order brace torque, V_{2nd}, is

$$V_{2nd} = \frac{2C_4 w_{1st} L \left(\Delta_{diaph}\right) \xi}{spa} \tag{17}$$

It should be noted that in calculating the shear forces resulting from the brace torque, not all of the torsion effects are included. Only the torsion effects in which the torsion is acting in the same direction on both purlins are included. For several of the second order torsion effects, the torsion at the eave acts opposite to the direction of the ridge, and thus the brace moments will balance without additional shear forces introduced to the purlin.

In Figure 8, the brace concentrated torsions are shown in the positive direction as they act on the purlin. When the torsion acting on the purlin is positive, as is when there is a large lateral deflection and correspondingly large second order torsions, the shear force generated in the brace results in a downward force on the ridge purlin and an uplift force on the eave purlin. Conversely, when the torsion acting on the purlin is negative, as is common when the diaphragm is relatively stiff, the shear forces in the braces generate an uplift force on the ridge purlin and a downward force in the eave purlin. This distinction is important because depending on the direction of the shear forces, it can provide rationale for either the ridge purlin or the eave purlin to fail first.

The shear forces required for equilibrium of the brace, as a result of the inclined principal axes of the purlin, cause an axial force, P_b, to be generated in the brace. Since the shear forces in each brace are largely equal and in the opposite direction, this axial force likewise is equal and opposite at each end of the brace. In Figure 8, the axial force generated is shown for the case when the brace torsion acts in the positive direction (the brace resists upslope rotation of the purlin).

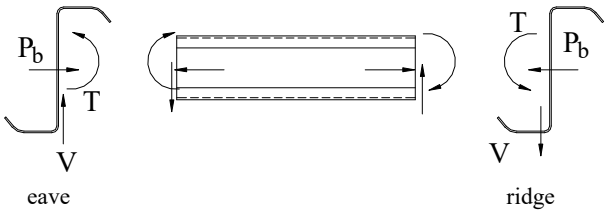

Figure 8. Brace shear transfer to purlin

To both calculate cross section stresses and evaluate the strength of the purlin, the moment about the orthogonal x-axis is calculated from the combination of uniformly applied forces, parabolic second order forces and shear forces generated at the braces. For simplification of the stress calculation, the moment effects due to the uniform and parabolically distributed loads are grouped separately from the moment caused by the shear forces in the brace. The moment about

the x-axis from the uniformly and parabolically distributed loads at any location, z, along the span is

$$M_{x,dist} = (w_{1st} + w_e)\left(\frac{L^2}{2}\right)\left(\frac{z}{L} - \left(\frac{z}{L}\right)^2\right) + w_{2nd}\left(\frac{L^2}{3}\right)\left(\left(\frac{z}{L} - 2\left(\frac{z}{L}\right)^3 + \left(\frac{z}{L}\right)^4\right)\right) \quad (18)$$

The moment about the x-axis resulting from the shear force in the brace is

When $z \le c$

$$M_{x,V} = (V_{1st} + V_{2nd})z \quad (19)$$

When $z \ge c$

$$M_{x,V} = (V_{1st} + V_{2nd})c \quad (20)$$

The total moment about the x-axis is the sum of the two moment effects

$$M_x = M_{x,dist} + M_{x,V} \quad (21)$$

For evaluating the strength, typically the critical locations to evaluate the moment are at the mid-span and at the brace location. The total moment about the x-axis at the mid-span ($z = L/2$) is

$$M_{x,mid} = (w_{1st} + w_e)\frac{L^2}{8} + w_{2nd}\frac{5L^2}{48} + (V_{1st} + V_{2nd})c \quad (22)$$

Similarly, the total moment about the x-axis at the brace location ($z = c$) is

$$M_{x,c} = (w_{1st} + w_e)\frac{c}{2}((L - c) + w_{2nd}\left(\frac{L^2}{3}\left(\frac{c}{L}\right)^4 - 2\left(\frac{c}{L}\right)^3 + \left(\frac{c}{L}\right)\right) + (V_{1st} + V_{2nd})c \quad (23)$$

Normal stresses from biaxial bending

Bending normal stresses are mapped on the cross section. For simplicity, applied forces are oriented along the orthogonal x- and y- axes perpendicular and parallel to the web respectively. There are 3 contributions to the bending stress: (1) the applied distributed force parallel to the web, (2) the distributed force provided by the sheathing perpendicular to the web, and (3) the shear force generated by the torsion brace. As previously discussed, the force generated in the sheathing is directly proportional to the applied force parallel to the web of the purlin by the factor σ. Because the shear forces generated by the torsion brace are equal and opposite on adjacent purlins, an axial force will be generated in the brace that balances the unsymmetric bending effects. Therefore, the stress distributions that result from the torsion brace shear forces will conform to the constrained bending distribution. The stresses are mapped according to the modified moments of inertia about the orthogonal x- and y- axes, I_{mx} and I_{my}, respectively introduced by Zetlin and Winter (1955).

$$I_{my} = \frac{I_x I_y - I_{xy}^2}{I_x} \quad (24)$$

$$I_{mx} = \frac{I_x I_y - I_{xy}^2}{I_y} \quad (25)$$

The bending stresses can be mapped at coordinates x and y across the purlin cross section by

$$f_{b,mid} = M_{x,dist} \cdot \left[\frac{-y}{I_{mx}} + \frac{x\frac{I_{xy}}{I_x}}{I_{my}} - \frac{x \cdot \sigma}{I_{my}} + \frac{y\frac{I_{xy}}{I_y}\sigma}{I_{mx}} \right] + M_{x,V}\left(\frac{-y}{I_x}\right) \tag{26}$$

Warping torsion stresses

The normal stresses caused by warping torsion, f_w, are calculated

$$f_w = E \cdot W_N \cdot \phi'' \tag{27}$$

where W_N is the normalized warping function at a specific point on the cross section and ϕ'' is the second derivative of the rotation function with respect to z due to the applied load. Guidance on calculating the normalized warping function for thin walled cross sections is provided in Cold-Formed Steel Design (Yu, 2010). The normalized warping function is calculated at the same coordinates (x, y) across the cross section as the bending normal stresses. As part of the section property calculator in CUFSM (Li and Schafer 2010), the normalized warping function is calculated.

There are 3 rotation functions to be considered: 1) uniform torsion along span, 2) parabolic distribution along span, 3) concentrated torque at brace locations (3rd points). The general rotation functions at any location, z, along the span are:

Uniform torsion

$$\phi_u'' = \frac{t_{1st}}{GJ}\left(\cosh\left(\frac{z}{a}\right) - \tanh\left(\frac{L}{2a}\right)\sinh\left(\frac{z}{a}\right) - 1\right) \tag{28}$$

Parabolic torsion distribution

$$\phi_p'' = \frac{t_{2nd}}{GJ}\left[\frac{8a^2}{L^2}\left(1 - \cosh\left(\frac{z}{a}\right) + \frac{\cosh\left(\frac{L}{a}\right) - 1}{\sinh\left(\frac{L}{a}\right)}\sinh\left(\frac{z}{a}\right)\right) + 4\left(\frac{z}{L}\right)^2 - 4\left(\frac{z}{L}\right)\right] \tag{29}$$

Concentrated torsion at brace location

$z < c$

$$\phi_{brace}'' = \frac{T_{1st} + T_{2nd}}{GJ}\left(\frac{1}{a}\right)\sinh\left(\frac{z}{a}\right)\left(\frac{\sinh\left(\frac{c}{a}\right) + \sinh\left(\frac{L-c}{a}\right)}{\tanh\left(\frac{L}{a}\right)} - \cosh\left(\frac{c}{a}\right) - \cosh\left(\frac{L-c}{a}\right)\right) \tag{30a}$$

$c < z < (L-c)$

$$\phi_{brace}'' = \frac{T_{1st} + T_{2nd}}{GJ}\left(\frac{1}{a}\right)\left[\sinh\left(\frac{z}{a}\right)\left(\frac{\sinh\left(\frac{c}{a}\right) + \sinh\left(\frac{L-c}{a}\right)}{\tanh\left(\frac{L}{a}\right)} - \cosh\left(\frac{L-c}{a}\right)\right) - \cosh\left(\frac{z}{a}\right)\sinh\left(\frac{c}{a}\right)\right] \tag{30b}$$

Combining equations 28, 29, and 30 into equation 27, the normal stress resulting from warping torsion at each coordinate on the cross section is calculated

$$f_w = E \cdot W_N \cdot \left(\phi_u'' + \phi_p'' + \phi_{brace}''\right) \tag{31}$$

Buckling analysis

The bending and warping normal stresses are combined at each location across the cross section. As CUFSM is used to perform the finite strip buckling analysis, each flat and radius of the cross section is divided into 4 segments, resulting in a total of 37 nodes along the cross section. The stress distribution is determined for each of the critical locations: the mid-span and the brace location as shown in Figure 9. For each stress distribution at the mid-span and brace location, the maximum stress, f_{max}, is determined. The maximum stress typically occurs in the radius between the top flange and the web as a result of biaxial bending and torsion effects. This stress will be below the yield stress and corresponds to the calculated moment, M_x. To normalize the stresses to the point of first yield, all of the stresses in the cross section are scaled up by the ratio of the yield stress, F_y, to the maximum stress, f_{max}. The yield moment about the x-axis, M_y, is calculated by multiplying the moment about the x-axis, M_x, by the ratio F_y/f_{max}. With the scaled stress distribution, CUFSM v4.05 is used to perform the finite strip buckling analysis. The local and distortional critical buckling moments, $M_{cr\ell}$ and M_{crd} respectively, are determined by multiplying the critical buckling load coefficients from CUFSM by the yield moment, M_y, about the x-axis. The nominal local buckling moment, $M_{n\ell}$, is calculated according to the provisions of AISI S100 Section F3.2 with the assumption that the compression flange is adequately braced to prevent global buckling and therefore, the nominal flexural stress for global buckling is the yield stress, $F_n = F_y$. Similarly, AISI S100 Section F4.1 is used to calculate the nominal flexural strength considering distortional buckling, M_{nd}.

The minimum between the local and distortional nominal strength is the nominal moment strength, M_n. This nominal moment strength is compared to M_x. If $M_n > M_x$, the strength is satisfied for the applied loading. Note, the calculated nominal strength in this case does not necessarily represent the actual strength. Because the process includes an approximation of second order effects, the stress distribution will change at different load levels. If the actual failure load is required, iteration is required by varying the applied load until M_n approximately equals M_x. Iteration may be terminated when M_n is within ten percent of M_x.

Global buckling

The global buckling strength is not explicitly calculated as the determination of the true global buckling strength is affected by the partial restraining effects of the sheathing. Three modes of global buckling can occur: 1) lateral buckling of the entire span between the inflection points, 2) lateral-torsional buckling of the middle span between the braces and 3) lateral-torsional buckling of the outer span between the inflection point and the brace. The analysis procedure to calculate the local and distortional buckling strength considers the diaphragm restraint provided by the sheathing when calculating the biaxial bending and torsion stresses and approximates member geometric second order effects as the purlin deflects laterally. The procedure conservatively ignores the additional torsional restraint provided by the sheathing. As such, the analysis essentially captures the mode of global buckling interacting with local buckling for the first two buckling modes. For typically configured paired torsion bracing systems, as the system deforms, there is sufficient restraint between the sheathing and braces to prevent substantial twisting of the purlin and thus force local buckling before lateral-torsional buckling can occur. This behavior model is supported by base tests, where the typically observed failure modes are either local or distortional buckling at the mid-span or brace location.

For typically configured paired torsion bracing systems, that is, systems with braces nominally near the third points, the third possible global buckling mode between the outer

inflection point and the first interior brace is unlikely to control the strength. For other configurations such that the distance between the inflection point and first interior brace is much longer than one third of the span length, the proposed procedure can be applied to this region of the span. It is recommended that the stresses be determined at the midpoint and 3/4 of the distance from the inflection point to the first interior brace.

In lieu of a more detailed lateral torsional buckling analysis, it is also recommended that the torsional braces be checked to verify that they have sufficient stiffness to prevent substantial twisting of the purlin. A stiffness limit for braces at the frame lines limiting the lateral deflection of the top of the purlin at the brace to a deflection of $\phi(d/20)$ for LRFD load combinations is required in AISI S100 Section I6.4. It is recommended that this same stiffness limit be applied to torsion braces along the span. For the maximum torsion in the brace, $T_{1st} + T_{2nd}$, the rotation of the purlin should be limited to $\phi(1/20)$ rad.

Comparison to base test

The analysis procedure was compared to the series of base tests performed by Emde (2010). The series of tests was performed with 3 tests each on 4 four purlin cross sections. A summary of the purlin cross section and span layout is shown in Table 1. The purlins were spaced at 5.0 feet, and the overall width of the panel was 7.0 feet allowing for 1.0 foot of panel overhang from the centerline of the web. The overall width of the chamber was 8.0 feet leaving a gap of 6 in. on each side of the panel.

Each system was tested utilizing the same diaphragm and clip configuration. The clip used was a "sliding tab" type with a thermal block at the base. The clip had a base to shoulder height of 2.375 in. and a thickness of the thermal block of 0.50 in. for a total clip height of 2.875 in. For a sliding tab clip, Seek and McLaughlin (2017) recommend that the effective standoff be 60 to 70 percent of the clip base to shoulder height. No explicit recommendations are made to accommodate a thermal block, but it was assumed to be virtually rigid which would increase the effective standoff. For calculations, the effective standoff distance was overestimated by taking 80 percent of the clip base to shoulder height (0.80 x 2.375 = 1.9) and added 0.5 in. to obtain an effective standoff distance rounded to 2.50 in. Initial analysis used a standoff distance of 0 in. The standoff distance of 2.50 in. showed better correlation to the test so, although the higher standoff distance was slightly overestimated, it is close to the actual value.

Table 1: Summary of evaluated base tests

Purlin Designation	Span (ft)	Brace Location, c (ft)	Diaphragm Stiffness, G' (lb/in.)
8Zx057	27.0	10.5	230
8Zx100	27.0	10.5	110
10Zx057	30.0	11.5	300
10Zx100	30.0	11.5	160

The diaphragm was modeled as described by Seek et al. (2016). As noted in this study, the more heavily loaded thicker purlins (0.100 in.) placed a larger demand on the diaphragm. Considering the non-linear shear behavior of standing seam panel systems, it is reasonable to consider the diaphragm to be more flexible as it is subject to higher demands. The diaphragm stiffness shown in Table 1 was chosen such that the predicted deflection of the system approximately matched the measured deflections. A comparison of the measured and predicted deflections are provided in Table 2.

Additionally in Table 2, the measured yield stress of each purlin, the uniform dead load, u_d, and the applied pressure at failure, u_p, are tabulated. It should be noted that in each test, the yield stress was only tested on the failed purlin. For calculations, it is assumed that, in each test, the purlin that did not fail has the same yield stress as the purlin that failed first.

For each test, the strength is predicted at four locations: the mid-span and brace location for both the "eave" and "ridge" purlin. At each location, M_{test} is the moment relative to the x-axis calculated from Eq. (22) for the midpoint location and Eq. (23) for brace point location. The cross section stresses at each location are determined, and the nominal flexural strength considering local and distortional buckling, $M_{n\ell}$ and M_{nd} respectively, is calculated. The smaller of the local or distortional strength is considered to be the controlling flexural strength, M_n. To compare the predicted flexural strength to the calculated strength from the test, the ratio M_{test}/M_n is calculated. The closer this value is to unity, the closer the method predicts the strength of the system. If the ratio is greater than 1, the predicted strength is less than the tested strength and is thus conservative. Conversely, if the ratio is less than one, the predicted strength is greater than tested and is unconservative. Considering each of the four locations investigated for a single test, the largest value of M_{test}/M_n is considered to be the overall controlling value, i.e. the location that should first experience failure and thus control the strength of the system. A summary of the calculated values for each test are provided in Tables 3 to 6. An overall comparison of the results of M_{test}/M_n is provided in Table 7.

Table 2: Base test applied loads and deflections

Purlin Designation	Test ID	u_d (psf)	u_p (psf)	F_y (ksi)	Δ_{mid} Tested (in.)	Δ_{mid} Predicted (in.)
8Zx057	1A	2.62	17.68	70.8	1.86	1.78
	1D	2.65	19.07	68.8	1.85	1.93
	1G	2.66	16.54	64.1	1.33	1.65
8Zx100	2D	3.18	37.65	79.1	6.17	5.97
	2E	3.18	27.15	79.1	5.29	4.27
	2F	3.20	37.87	79.1	5.94	5.93
10Zx057	3A	2.84	19.46	56.1	1.18	1.74
	3D	2.82	18.54	68.3	1.53	1.59
	3E	2.82	16.55	63.9	1.49	1.37
10Zx100	4A	3.46	45.02	67.1	5.59	5.72
	4C	3.47	40.02	65.8	5.75	5.06
	5A	3.47	44.57	65.4	4.72	4.96

Results for 8Zx057

Comparison of the predicted strength versus the tested strength of the 8Zx057 purlins are shown in Table 3. In Table 3, the purlin location (eave or ridge) that failed first is indicated with bold text and the predicted location of failure is indicated by shaded text enclosed in a box. Consistently, the predicted local buckling strength is 5 to 10 percent greater than the distortional buckling strength. Thus, in all tests the eave purlin at mid-span was predicted to fail first by distortional buckling and the predicted moment is in line with the failure moment. Although for each test, the exact failure mode was not reported by Emde, the most common failure mode was reported to be distortional buckling at mid-span. For test 1D, the ridge purlin failed first which

was not predicted. However, the difference in M_{test}/M_n between the eave and ridge purlin is small (1.11 versus 1.06).

Results for 8Zx100

The comparison of the predicted strength versus the tested strength of the 8Zx100 purlins is shown in Table 4. Consistently, the predicted distortional buckling strength is less than the local buckling strength and therefore will control the strength. In all cases, the predicted mode of failure is distortional buckling at the ridge brace location. However, in all tests, the failure actually occurred at the eave purlin although the actual location (mid-span or brace location) was not reported. Test 2E failed at a load level significantly lower than both the other two tests and lower than predicted. Emde reported that premature failures occurred in several tests as a result of failures in the connection between the torsional brace and the purlin. It is believed that connection failure is the result of the lower supported load in Test 2E. It should also be noted that in the evaluation of the predicted strength, it is assumed that the torsional brace is perfectly rigid. If the brace is modeled as flexible, the moments in the brace are reduced along with the balancing shear forces. This change in the shear forces can shift the predicted location of failure from the ridge to the eave.

Table 3: Summary of results: 8Zx057

Test ID	Location	M_{test} (k-ft)	F_y/f	Local Ld. Factor	Dist. Ld. Factor	$M_{n\ell}$ (k-ft)	M_{nd} (k-ft)	M_n (k-ft)	M_{test}/M_n
1A	**Eave: Mid-Span**	7.04	1.46	0.60	0.67	7.34	6.88	6.88	1.02
	Eave: Brace	6.68	1.53	0.62	0.66	7.40	6.82	6.82	0.98
	Ridge: Mid-Span	6.74	1.59	0.64	0.61	7.86	6.95	6.95	0.97
	Ridge: Brace	6.41	1.67	0.67	0.60	7.94	6.86	6.86	0.93
1D	Eave: Mid-Span	7.52	1.32	0.62	0.71	7.16	6.79	6.79	1.11
	Eave: Brace	7.14	1.39	0.65	0.67	7.28	6.64	6.64	1.07
	Ridge: Mid-Span	7.23	1.44	0.66	0.63	7.72	6.84	6.84	1.06
	Ridge: Brace	6.88	1.51	0.70	0.61	7.81	6.70	6.70	1.03
1G	**Eave: Mid-Span**	6.66	1.39	0.67	0.73	6.90	6.44	6.44	1.03
	Eave: Brace	6.33	1.47	0.68	0.73	6.93	6.44	6.44	0.98
	Ridge: Mid-Span	6.34	1.47	0.67	0.73	6.90	6.45	6.45	0.98
	Ridge: Brace	6.03	1.54	0.68	0.73	6.94	6.44	6.44	0.94

Table 4: Summary of results: 8Zx100

Test ID	Location	M_{test} (k-ft)	F_y/f	Local Ld. Factor	Dist. Ld. Factor	$M_{n\ell}$ (k-ft)	M_{nd} (k-ft)	M_n (k-ft)	M_{test}/M_n
2D	**Eave: Mid-Span**	13.07	1.27	1.72	1.90	16.61	15.96	15.96	0.82
	Eave: Brace	12.31	1.23	2.54	1.52	15.13	13.60	13.60	0.91
	Ridge: Mid-Span	14.69	1.13	1.76	1.68	16.63	15.40	15.40	0.95
	Ridge: Brace	14.07	1.10	2.30	1.45	15.55	13.76	13.76	1.02
2E	**Eave: Mid-Span**	9.96	1.67	1.73	1.71	16.63	15.49	15.49	0.64
	Eave: Brace	9.41	1.66	2.22	1.50	15.62	13.97	13.97	0.67
	Ridge: Mid-Span	10.62	1.59	1.68	1.65	16.91	15.58	15.58	0.68
	Ridge: Brace	10.15	1.59	2.06	1.49	16.09	14.37	14.37	0.71
2F	**Eave: Mid-Span**	13.15	1.29	1.71	1.83	17.01	16.17	16.17	0.81
	Eave: Brace	12.39	1.26	2.48	1.51	15.66	14.04	14.04	0.88
	Ridge: Mid-Span	14.77	1.14	1.70	1.69	16.80	15.60	15.60	0.95
	Ridge: Brace	14.15	1.11	2.22	1.46	15.74	13.97	13.97	1.01

Results for 10Zx057

The results comparing the predicted strength versus the tested strength of the 10Zx057 purlins are shown in Table 5. Like previous tests, for Tests 3D and 3E, the distortional buckling strength is less than the local buckling strength and therefore predicted to control. For test 3A however, the local buckling strength is less than the distortional buckling strength. Emde reported lip local buckling to be one of the observed modes of failure. In all cases the eave purlin was predicted to fail first which matched the behavior observed in the tests. In all cases, M_{test}/M_n is conservative, but not overly so.

Results for 10Zx100

The results comparing the predicted strength versus the tested strength of the 10Zx100 purlins are shown in Table 6. In all cases, the distortional buckling strength is less than the local buckling strength and thus controls the overall strength of the purlin. It should be noted that at the mid-span location, the distortional buckling strength is fairly close to the local buckling strength. However, at the brace location, due to the significant change in the distribution of the stresses (see Figure 9) as a result of the concentrated brace torque, there is a significant drop in the distortional buckling strength relative to the local buckling strength. In all cases, the ridge purlin is predicted to fail at the brace location. In the tests, the ridge purlin was the first to fail although the exact location along the span was not reported. In all cases the predicted strength was less than the tested strength, thus providing a conservative predicted strength.

Like the tests on the 8Zx100 purlins, the 10Zx100 purlins placed large demands on the torsion braces. Although the braces were modeled as rigid, it is likely that they did not behave as rigid. As flexibility of the brace is introduced, the brace moments and the balancing shear forces decrease. This change in the shear force will decrease M_{test} for the ridge purlin and bring the ratio of M_{test}/M_n closer to unity.

Table 5: Summary of results: 10Zx057

Test ID	Location	M_{test} (k-ft)	F_y/f	Local Ld. Factor	Dist. Ld. Factor	$M_{n\ell}$ (k-ft)	M_{nd} (k-ft)	M_n (k-ft)	M_{test}/M_n
3A	**Eave: Mid-Span**	9.59	1.29	0.52	0.71	8.42	8.49	8.42	1.14
	Eave: Brace	9.05	1.38	0.54	0.68	8.65	8.46	8.46	1.07
	Ridge: Mid-Span	9.07	1.45	0.47	0.66	8.64	8.77	8.64	1.05
	Ridge: Brace	8.59	1.55	0.48	0.64	8.80	8.76	8.76	0.98
3D	**Eave: Mid-Span**	9.18	1.61	0.40	0.48	9.16	8.67	8.67	1.06
	Eave: Brace	8.67	1.72	0.42	0.47	9.43	8.69	8.69	1.00
	Ridge: Mid-Span	8.68	1.78	0.42	0.52	9.76	9.37	9.37	0.93
	Ridge: Brace	8.22	1.90	0.43	0.50	9.94	9.32	9.32	0.88
3E	**Eave: Mid-Span**	8.34	1.67	0.44	0.46	8.96	8.05	8.05	1.04
	Eave: Brace	7.87	1.75	0.46	0.45	9.00	7.89	7.89	1.00
	Ridge: Mid-Span	7.84	1.80	0.41	0.55	8.82	8.74	8.74	0.90
	Ridge: Brace	7.42	1.91	0.42	0.53	8.97	8.68	8.68	0.85

Table 6: Summary of results: 10Zx100

Test ID	Location	M_{test} (k-ft)	F_y/f	Local Ld. Factor	Dist. Ld. Factor	$M_{n\ell}$ (k-ft)	M_{nd} (k-ft)	M_n (k-ft)	M_{test}/M_n
4A	Eave: Mid-Span	19.36	1.12	1.28	1.48	19.99	19.34	19.34	1.00
	Eave: Brace	18.13	1.10	1.81	1.26	19.91	16.83	16.83	1.08
	Ridge: Mid-Span	21.35	1.02	1.26	1.49	19.97	19.45	19.45	1.10
	Ridge: Brace	20.37	1.01	1.61	1.33	20.31	17.65	17.65	1.15
4C	Eave: Mid-Span	17.54	1.23	1.24	1.35	19.71	18.70	18.70	0.94
	Eave: Brace	16.44	1.23	1.68	1.18	20.18	16.68	16.68	0.99
	Ridge: Mid-Span	18.96	1.14	1.23	1.36	19.71	18.80	18.80	1.01
	Ridge: Brace	18.07	1.14	1.54	1.23	20.11	17.27	17.27	1.05
5A	Eave: Mid-Span	19.20	1.11	1.28	1.48	19.61	18.97	18.97	1.01
	Eave: Brace	17.98	1.09	1.84	1.29	19.55	16.66	16.66	1.08
	Ridge: Mid-Span	21.16	1.01	1.29	1.60	19.68	19.46	19.46	1.09
	Ridge: Brace	20.19	1.00	1.63	1.43	20.01	17.74	17.74	1.14

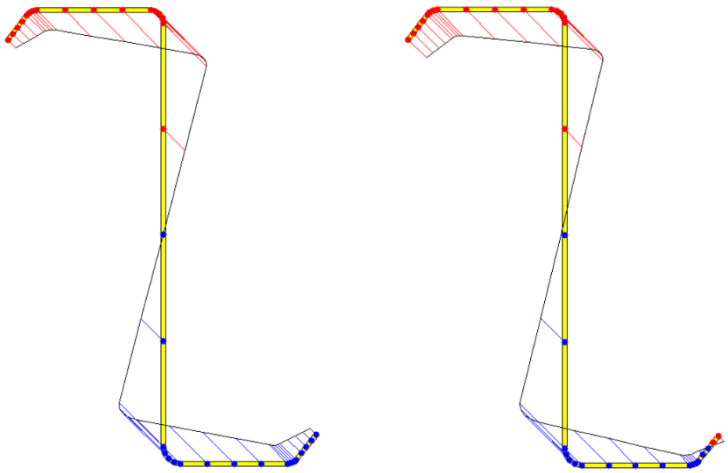

(a) mid-span (b) brace location

Figure 9. Distribution of normal stresses

Summary of base test results

A summary of all analytical comparisons to the test results is provided in Table 7. Results are organized by test, summarizing the ratio of M_{test}/M_n at each investigated location. On the right side of the table, the controlling value for M_{test}/M_n for each test is shown in addition to the average value for the series of tests for each profile and the coefficient of variation. For each test, the purlin failing first is designated by shaded cells and the location predicted to fail first is indicated by a bold outline and bold text. In all but one test, the predicted strength is less than the tested strength, indicating a conservative prediction of strength. The one case that did not conform with the rest of the results, test 2E, it is believed failed prematurely as a result of the failure of the torsion brace connection. Eliminating this one anomaly, the overall average of M_{test}/M_n is 1.07.

In most cases, the methodology was able to predict whether the eave or ridge purlin failed first, with two major exceptions. The first exception was for test 2D where the difference in predicted strength between the eave and ridge purlin was small and could have been as a result of the assumed yield strength of the eave purlin. The second exception is for tests 2D, 2E, and 2F. In these tests, failure occurred in the eave but was predicted at the ridge. The braces were modeled as rigid, however, if modeled as flexible, the brace moments and corresponding shear forces decrease, decreasing the moment at the ridge and increasing the moment at the eave. Correspondingly this could shift the predicted location of failure from the eave to the ridge.

Table 7: Summary of Mtest/Mn

	Eave		Ridge		Controlling	Average	COV
Test ID	Midpoint	Brace Point	Midpoint	Brace Point	Value		
1A	**1.02**	0.98	0.97	0.93	1.02	1.054	0.04
1D	**1.11**	1.07	1.06	1.03	1.11		
1G	**1.03**	0.98	0.98	0.94	1.03		
2D	0.82	0.91	0.95	**1.02**	1.02	0.914	0.16
2E	0.64	0.67	0.68	**0.71**	0.71		
2F	0.81	0.88	0.95	**1.01**	1.01		
3A	**1.14**	1.07	1.05	0.98	1.14	1.078	0.04
3D	**1.06**	1.00	0.93	0.88	1.06		
3E	**1.04**	1.00	0.90	0.85	1.04		
4A	1.00	1.08	1.10	**1.15**	1.15	1.113	0.04
4C	0.94	0.99	1.01	**1.05**	1.05		
5A	1.01	1.08	1.09	**1.14**	1.14		

Diaphragm stiffness for strength evaluation

The strength of Z-purlin roof systems is a function of the stiffness of the diaphragm. The stiffness of the diaphragm affects the lateral restraint force provided by the sheathing – in general the greater the stiffness of the diaphragm, the larger the force interacting between the purlin and the diaphragm. This in-plane force in the diaphragm has a large impact both on biaxial bending stresses and the torsion that the purlin is subjected to. Additionally, second order effects are driven by the lateral deflection of the diaphragm and can significantly impact the strength of a purlin system.

The shear behavior of standing seam diaphragms typically exhibits non-linear behavior with an initial stiffness approximately linear then softening with increase shear force. The load-deflection behavior of a standing seam diaphragm as tested according to the Cantilever Test Method (AISI 2017b), is shown in Figure 10. Two test curves are shown. The lower curve shows the tested load-deflection behavior of the standing seam panel systems without typical eave fastening – meant to represent the stiffness of the "field" of the diaphragm. The typical eave fastening mechanism in in-situ roof systems provides resistance to seam slippage and therefore increases the diaphragm stiffness. The upper curve shows the tested load-deflection behavior of the standing seam panel system tested with the typical eave attachment. The stiffness of diaphragm systems, G', is calculated based on the linear behavior up to the 40 percent of the maximum force sustained by the diaphragm to capture the initial linear stiffness. This stiffness is shown in Figure 10 for the diaphragm tested without eave attachment.

In the previous section, the calculated lateral deflection of the diaphragm was compared to the measured lateral deflection in the series of base tests. As thicker purlins place greater demands on the diaphragm, the stiffness of the diaphragm effectively decreases. Plotted in Figure 10 are lines representing the diaphragm stiffness used in the strength prediction calculations that were calibrated from measured lateral deflection in the base tests. The end points of the lines represent the peak shear in diaphragm if behaving linearly.

The base tests were performed with a 1 in. x 1 in. x ¼ in. angle fastened along each of the panel

ends. This angle helps to prevent spreading of the seams at the panel end and premature failure of the panel. This end attachment also helps to restrict seam movement, so it is expected that this attachment will increase the diaphragm stiffness relative to the "field" stiffness of the diaphragm.

Comparing the calibrated stiffness used in the strength prediction calculations, as shown in Figure 10, the stiffness of all cases is less than that predicted for the "field" diaphragm by the cantilever test method (467 lb/in.), even considering that the stiffness should be increased by the edge angle attachments. For the thinner purlins (10Zx057 and 8Zx057), the predicted linear diaphragm stiffness is 300 lb/in. and 230 lb/in. respectively. The predicted peak shear in the "field" diaphragm from the cantilever base test is 68 lb/ft. The peak shear force predicted for the 10Zx057 and 8Zx057 tests is 69.6 lb/ft and 61.0 lb/ft respectively. These diaphragm shear forces are in the range of the peak shear force in the tested diaphragm without eave attachment. The total shear demand for the 10Zx057 purlin is greater than for the 8Zx057 purlin. It would be expected that as a result of the higher net shear demand in the 10Zx057 system, the calibrated stiffness would be less. The 10Z purlins were tested on a longer span than the 8Z purlins, which ultimately has some effect on the predicted stiffness/shear demand.

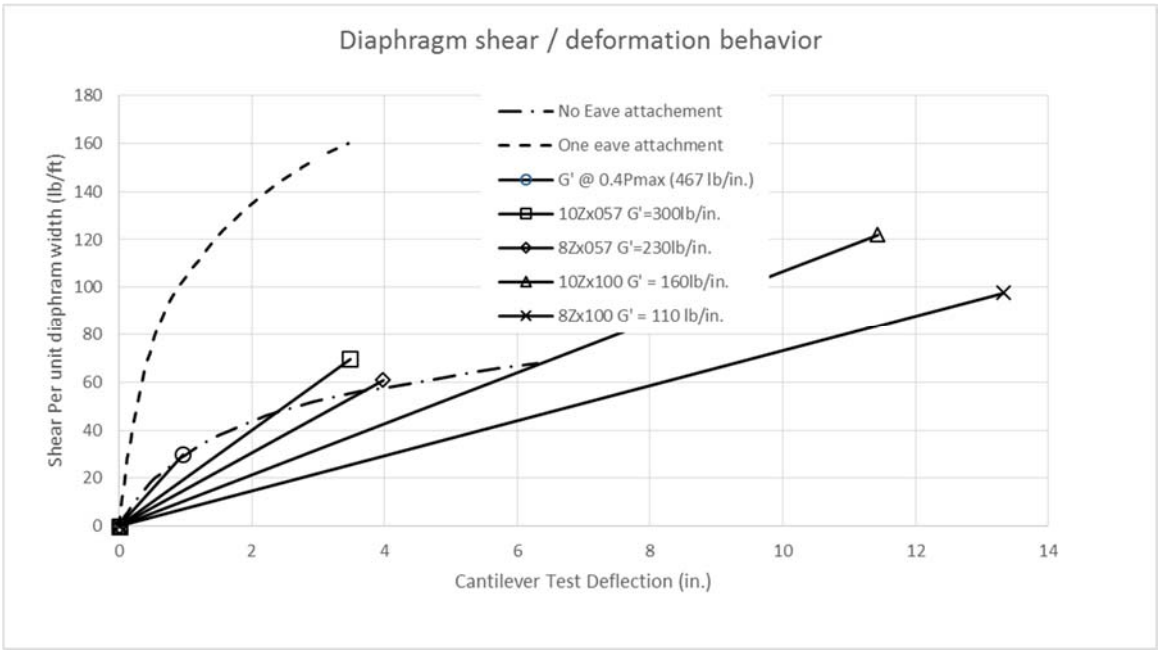

Figure 10. Comparison of diaphragm stiffness

The thicker purlins put much larger demands on the diaphragm. Assuming a linear stiffness, the calibrated stiffness of the 10Zx100 purlin is 160 lb/in. while the stiffness of the 8Zx100 purlin is 110 lb/in. Extending this stiffness to the maximum predicted shear demand in the diaphragm (121.1 lb/ft for 10Zx100 tests and 97.7 lb/ft for the 8Zx100 tests) extends the curves well beyond the tested range from the cantilever test.

To get to the true behavior of the diaphragm as it interacts with the purlin will likely require the diaphragm to be analyzed as non-linear. Additionally, near the ends of the spans where the shear demand is higher, there is likely slippage occurring between the clip and the panel. Both of these effects have the potential to reduce the peak shear demand calculated in the sheathing. Additional work is required to better understand this behavior. It is a reasonable and conservative approximation to calibrate the stiffness of the diaphragm from base tests and use the linear stiffness in predicting the strength.

Analysis of purlins in sloped roof systems

The previous section has shown that the methodology is effective in not only predicting the capacity of purlins in roof systems with paired torsion braces, but also predicts some of the nuances such as failure away from the mid-span at the brace location and failures at the ridge versus the eave purlin. As the methodology is applied to real systems there are several important modifications. First, for real systems, they are not subject to some of the load imbalances inherent in the base test. Additionally, in the base test, although the purlins are typically spaced at 5 feet, the panel width is typically only 7 feet so the depth of diaphragm tributary to each purlin is only 3.5 feet. In a real system, with purlins spaced at 5 feet the depth of diaphragm tributary to each is 5 feet, which effectively increases the diaphragm stiffness relative to the purlin. And finally, slope effects must be considered in real roof systems. As shown in Figure 11, as the slope of the roof increases, the lateral deflection changes, shifting from an upslope translation to a downslope translation at higher slopes. These downslope forces generated can substantially change the distribution of stresses in the cross section. Figure 12 shows the difference in stress distribution between 0:12, 2:12 and 4:12 slopes.

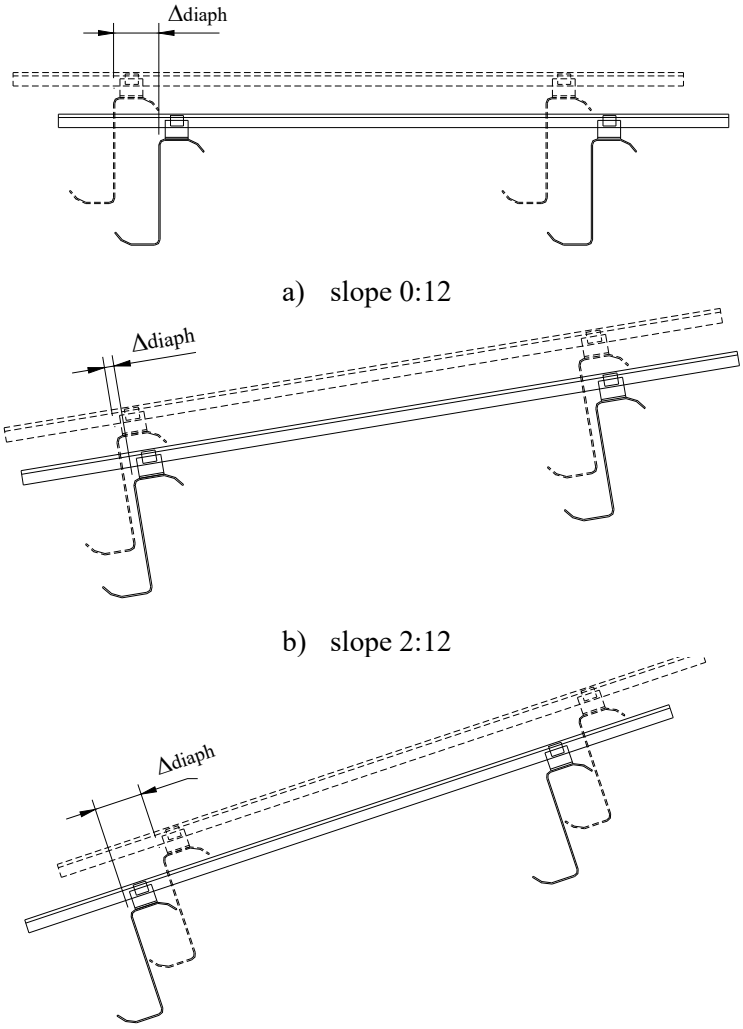

a) slope 0:12

b) slope 2:12

c) slope 4:12

Figure 11. Variation of diaphragm deflection with roof slope

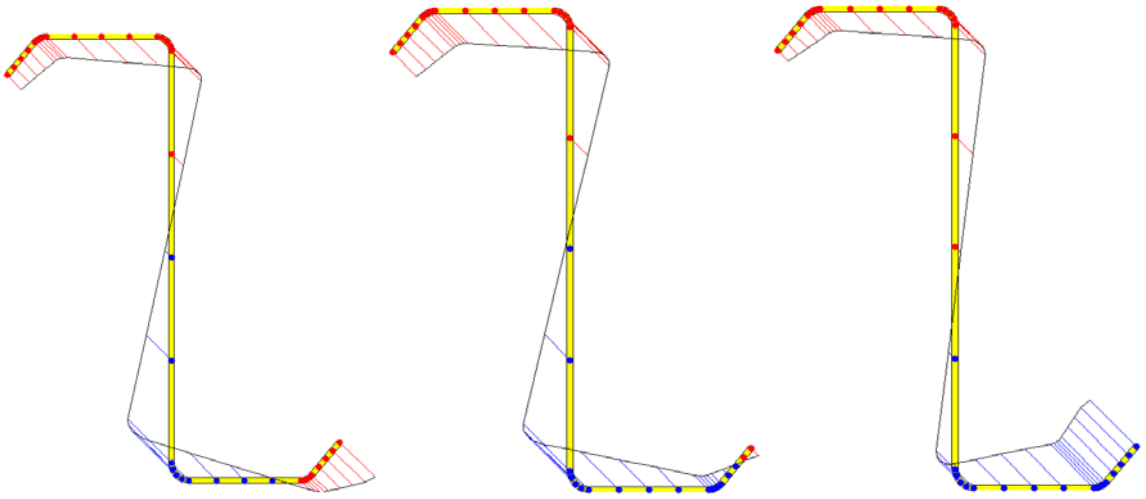

a) slope 0: 12 b) slope 2:12 c) slope 4:12

Figure 12. Variation in stress distribution with varied slope

There are several changes that are made to the analysis procedure when evaluating real systems. The first major change is with the proportion of the applied load that results in a uniform force in the diaphragm. Previous applications of the component stiffness method Murray et al. (2009) from which the methodology is based defined the term, σ, as the proportion of the distributed force applied in the *gravity* direction that results in a distributed force in the diaphragm. When determining the cross section stresses in a sloped roof system, it is more meaningful to define the term, ρ, as the proportion of the distributed force applied perpendicular to the sheathing (parallel to the web) that results in a distributed force in the diaphragm. This simplifies the procedure for both gravity and uplift loads. As was noted in the previous section, the change in terminology is used to make a distinction between flat roof systems (as with the base test) and sloped roof systems. For a flat roof system, gravity is directed perpendicular to the sheathing, therefore σ and ρ will have the same result in this case.

The procedure for evaluating purlins in real roof systems follows the same pattern as described previously for evaluating the base test. The equations for evaluating both simple span systems and the interior span in a multi-span system (fixed-fixed end conditions) are provided in Appendix 1. The procedure is outlined below.

1. Calculate ρ, the proportion of the load perpendicular to sheathing that results in a uniform force between the purlin and diaphragm in the plane of the diaphragm. The term w_{rest} represents the uniform force transferred between the purlin and diaphragm along the span.
2. Calculate the mid-span lateral displacement of the diaphragm, Δ_{mid}
3. Calculate the torsion effects on the purlin. Note that torsion effects are simplified for real systems because they are not subject to some of the load imbalances inherent in the base test. The torsion effects include
    a. Uniformly distributed first order torsion, t_{1st}, resulting from the applied load acting eccentrically on the flange of the purlin, and the lateral restraint provided by the sheating acting at the effective standoff distance.

b. Parabolically distributed second order torsion, t_{2nd}, resulting from the lateral deflection of the system of purlins.

4. Calculate the concentrated restraining torque at the torsion brace locations considering first order effects, T_{1st}, and second order effects, T_{2nd}. This restraing torque is calculated by displacement compatibility between the torsion braces and the purlin at the brace location. The torsion braces are assumed to be rigid.
5. Calculate additional interacting forces between the purlin and the braces to maintain equilibrium of the braces. The moments at each end of the torsion brace are balanced by shear forces, V, as shown in Figure 8 that must be resisted by the purlin. The shear forces transferred to the purlin result in a small axial force, P_b, in the brace as the result of the asymmetric bending of z-purlins.
6. At each critical location along the span of the purlin, calculate the nominal local and distortional buckling flexural strength, $M_{n\ell}$ and M_{nd} respectively. The critical locations to calculate the strength are the mid-span location and brace location.
    a. Calculate the moment about the x-axis, M_x.
    b. Calculate the biaxial bending stresses in the purlin cross section, f_b.
    c. Calculate the warping torsion normal stresses, f_w, in the purlin cross section resulting from the uniformly distributed torsion, parabolically distributed torsion and the concentrated torque at the brace locations.
    d. Sum the bending stresses and warping stresses at each location across the cross section and find the maximum stress in the cross section, f_{max}.
    e. Scale the stresses in the cross section to first yield by multiplying the stress at each location by the factor F_y/f_{max}.
    f. Scale the moment about the x-axis, M_x, with the same stress scale factor (F_y/f_{max}) to determine the yield moment, M_y.
    g. Perform finite strip buckling analyis (CUFSM) using the scaled stresses along the cross section. From the signature curve, determine the respective local and distortional buckling load factors.
    h. Calculate the critical local and distortional buckling moments, $M_{cr\ell}$ and M_{crd}, respectively, as the product of the buckling load factor and the yield moment, M_y.
    i. Calculate the nominal local buckling moment, $M_{n\ell}$, according to AISI S100 Section F3.2 with $F_n = F_y$. As stresses are calculated considering the biaxial bending effects of interaction with the sheathing and second order torsion effects, this calculation is an approximation of the local buckling interacting with global buckling strength.
    j. Calculate the nominal distortional buckling moment, M_{nd}, according to AISI S100 Section F4.1.
    k. The nominal moment strength, M_n, is the minimum of the local and distortional buckling strength at the location being investigated.
    l. Compare the nominal moment strength to moment about the x-axis at the location being investigated. If $M_n > M_x$, the purlin has sufficient capacity at the checked location to support the uniform load. Note, the calculated nominal strength in this case does not necessarily represent the actual strength. Because the process includes an approximation of second order effects, the stress distribution will change at different load levels. If the actual failure load is required, iteration is required by varying the applied load until $M_n \approx M_x$. Iteration may be terminated

when M_n is within ten percent of M_x.

7. Compare the ratio of M_x/M_n at each of the critical locations along the span. The maximum ratio of M_x/M_n provides the location that will control the strength of the design.

Predicted strength of sloped roofs

Historically, the philosophy of the design of sloped roof systems has been to determine the strength of the purlin system in a flat roof condition using the base test and any slope effects are resisted by the anchorage system. The lateral deflection of the system is limited to L/360 for most systems and L/180 for systems with torsion braces. While this approach is generally considered to be conservative, it is hypothesized that increased capacity can be realized by including slope effects to evaluate the actual strength. It is also desirable to relax the lateral deflection limits, which is reasonable when the strength of the purlin directly incorporates the effects of lateral deformations.

To test this hypothesis, a system of purlins was evaluated on slopes varying from a 0:12 pitch to a 4:12 pitch. To provide a baseline for comparison, the system of purlins evaluated is the same as used in this report for the base test evaluation. From the series of tests, two purlins were evaluated: an 8Zx057 (Test ID 8Z16-1A) and an 8Zx100 (Test ID 8Z12-2D). The measured cross section dimensions reported by Emde (2010) were used. The purlins were analyzed in a multi-span condition (fixed-fixed ends) with the purlin span, L = 27 feet, and the torsion braces spaced at c = 10.5 feet from the ends. The diaphragm stiffness values were the same as used in the base test evaluation. Test parameters are summarized in Table 8.

Table 8. Purlin System Analysis Parameters

Purlin	F_y (ksi)	G′ (lb/in.)	standoff, s (in.)	eccentricity, e_{sx} (in.)
8Zx057	70.8	230	2.5	1/3b = 0.643
8Zx100	79.1	110	2.5	1/3b = 0.665

The relationship between the predicted maximum supported uniform load in the gravity direction and roof slope is shown in Figure 13 for the 8Zx057 purlin and in Figure 14 for the 8Zx100 purlin. The maximum supported uniform load is used as a comparison rather than the moment at failure because the moment at failure fluctuates considerably as a result of the brace shear. In both Figure 13 and Figure 14, the strength predicted by the R-factor derived from the base test is also plotted as a base line. The small increase in the supported uniform load derived from the base test with increasing roof slope results from the subdivision of the gravity load into components perpendicular and parallel to the plane of the sheathing. For the 8Zx057 purlin, at the flat roof condition, the strength predicted from the Direct Strength method is slightly less than that predicted by the base test. The strength predicted from the base test is extrapolated from a simple span configuration to the multi-span fixed-fixed configuration. The fixed-fixed condition requires a larger uniform loading to reach the equivalent mid-span moment of the fixed-fixed condition. When analyzed using the proposed direct strength method, the larger uniform loading required to reach the equivalent mid-span simple span moment causes larger lateral deflection which in turn results in increased predicted biaxial bending stresses. The increased stresses shift towards the web, predicting local buckling of the web. In Table 9, the calculated local and distortional buckling load factors at both the mid-span and brace location are provided, as well as the predicted maximum supported load predicted from the buckling load factors with the

controlling load highlighted. Table 9 also reports the uniform load equivalent to the base test R-factor as well as the predicted buckling load factors from the base test for comparison to the sloped multi-span system results. Table 10 presents the stress scale factors, predicted failure mode and location, as well as the lateral deflection of the system.

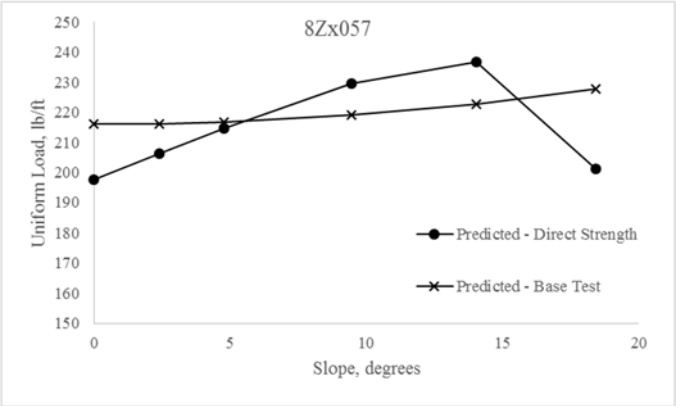

Figure 13. Maximum uniform load versus roof slope, 8Zx057

As the slope of the roof system increases, and the downslope component of the gravity load begins to contribute downslope forces to the diaphragm, the lateral deflection of the purlins decreases. Correspondingly, the brace moments decrease as second order torsion decreases and the stress scale factor increases, indicating the redistribution of stresses away from the web. The supported uniform load increases as a result of the change in distribution of stresses. With increasing slopes, the failure mode changes. At slopes higher than a 3:12 pitch, the lateral deflection of the purlin transitions downslope. The lateral bending effect in this case shifts stresses towards the flange tips. The combination of lateral bending and concentrated torsion at the brace location causes the failure mode to shift to local buckling of the flange stiffener at the brace location. This shift in stresses causes the supported uniform load to rapidly decline. However, in this case, peak stresses occur in the tension flange, so additional strength may be realized by considering inelastic reserve capacity.

Table 9. Buckling load factors and maximum uniform loads for 8Zx057 purlin

	Buckling Load Factors				Uniform Load (lb/ft)				
	Mid-span		Brace		Mid-span		Brace		Min.
	Local	Dist.	Local	Dist.	Local	Dist.	Local	Dist.	
Base Test	0.60	0.67	0.62	0.66	-	-	-	-	216
0:12	0.59	1.02	0.92	0.83	198	218	230	203	198
0.5:12	0.59	0.93	0.85	0.78	206	220	242	214	206
1:12	0.58	0.85	0.78	0.74	215	223	255	227	215
2:12	0.58	0.71	0.61	0.67	237	230	285	266	230
3:12	0.58	0.59	0.52	0.82	262	237	241	257	237
4:12	0.70	0.59	0.63	1.00	261	221	201	216	201

Table 10. Analysis comparisons 8Zx057 purlin

	Max w_n (lb/ft)	F_n/F_y	Failure			Brace Moment (lb-ft)	Deflection	
			Up/Down	Location	Mode		Lateral (in.)	Ratio L/
Base Test	216	1.457	Downhill	Mid	Dist.	387	1.86	174
0:12	198	1.406	Uphill	Mid	Local	2935	2.78	117
0.5:12	206	1.406	Uphill	Mid	Local	2474	2.45	132
1:12	215	1.414	Uphill	Mid	Local	1895	2.09	155
2:12	230	1.457	Uphill	Mid	Dist.	305	1.24	260
3:12	237	1.578	Uphill	Mid	Dist.	-1529	0.28	1166
4:12	201	1.374	Downhill	Brace	Local	-2675	-0.59	553

The relationship between the roof slope and the supported uniform load as shown in Figure 14 for 8Zx100 is similar to that of the 8Zx057 purlin. At the flat slope, the strength predicted by the direct strength method is less than that predicted by the base test R-factor. With increasing slope, the strength predicted by the direct strength method increases with a maximum at a pitch of approximately 3:12, then begins to dramatically decrease. Although the overall trends between the thicker and thinner purlin are similar, the predicted behavior as summarized in Tables 11 and 12 for the 8Zx100 purlin is different. For the thicker purlin, the large lateral deflections cause substantial second order torsions which causes large torsion brace moments. The predicted failure mode is distortional buckling at the brace location.

As the slope increases, the second order torsion decreases and the predicted supported uniform load increases. Similar to the thinner purlin, as the lateral deflection of the purlin transitions downslope at pitches greater than 3:12, the predicted strength decreases. As for the thin purlin, the tension stresses are significantly higher than the compression stresses, so additional strength can likely be realized by considering inelastic reserve capacity.

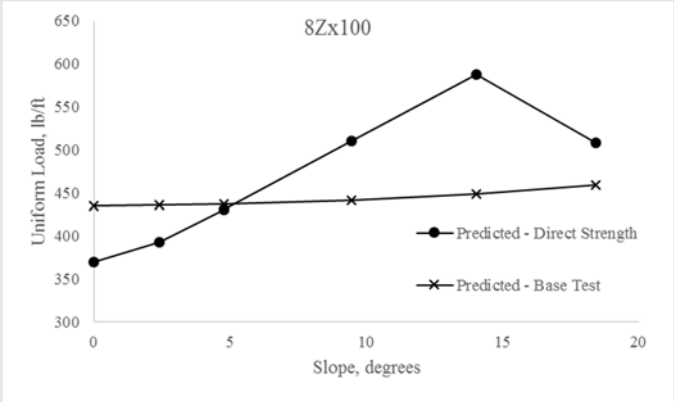

Figure 14. Maximum uniform load versus roof slope, 8Zx100

Table 11: Buckling load factors and maximum uniform loads for 8Zx100 purlin

	Buckling Load Factors				Uniform Load (lb/ft)				
	Mid-span		Brace		Mid-span		Brace		Min.
	Local	Dist.	Local	Dist.	Local	Dist.	Local	Dist.	
Base Test	1.72	1.90	2.54	1.52	-	-	-	-	435
0:12	1.59	N/A	3.21	2.07	437	N/A	376	370	370
0.5:12	1.59	3.5	3.1	1.86	466	472	412	393	393
1:12	1.58	2.43	2.83	1.7	498	506	464	431	431
2:12	1.57	1.74	2.41	1.35	581	553	590	511	511
3:12	1.55	1.18	1.57	1.16	696	588	824	689	588
4:12	1.94	1.02	1.73	1.88	692	543	530	508	508

Table 12: Analysis comparisons 8Zx100 purlin

			Failure				Deflection	
	Max w_n (lb/ft)	F_n/F_y	Up/Down	Location	Mode	Brace Moment (lb-ft)	Lateral (in.)	Ratio L/
Base Test	435	1.105	Uphill	Brace	Dist.	5362	6.17	53
0:12	370	1.017	Uphill	Brace	Dist.	13777	5.44	60
0.5:12	393	1.048	Uphill	Brace	Dist.	12977	4.95	65
1:12	431	1.075	Uphill	Brace	Dist.	11419	4.30	75
2:12	511	1.156	Uphill	Brace	Dist.	8541	3.30	98
3:12	588	1.210	Downhill	Mid-	Dist.	-28	1.21	268
4:12	508	1.044	Downhill	Brace	Dist.	-8796	-1.00	323

It should be noted for both of the purlins evaluated, at low slopes, the predicted lateral deflections do not satisfy the L/180 lateral deflection limit. If the roofing system and its external connections are able to accommodate the predicted deflections, it is reasonable to relax the lateral deflection limit for deflections calculated for strength limit states. It should also be noted that the predicted demands on the torsion braces can be much higher in a sloped roof system than is tested in the base test method. This additional demand should be considered when extrapolating the base test method to sloped roof systems.

Conclusions

A methodology is presented that uses the Direct Strength Method to predict the local and distortional buckling strength of Z-sections in roof systems with one flange connected to sheathing and paired torsion braces along the span. The methodology considers the diaphragm interaction between the purlin and sheathing as well as the restraint provided by the torsional braces to calculate the biaxial bending and torsion stresses in the cross section. These stresses can vary substantially from the traditionally assumed constrained stress distribution which in turn impacts the predicted strength.

To validate the methodology, it is compared to a series of base tests. The correlation between the base tests and the methodology is good and provides a conservative approximation of the strength. The methodology is able to provide rationale and predict a buckling failure away from the mid-span at the brace location as well as predict the failure of the eave purlin versus the ridge

purlin in the base test.

The methodology is also adapted to evaluate sloped roof systems. Equations are provided for both simple span and multi-span interior roof systems. There are several small differences and simplifications that can be made for evaluating these real systems versus base tested systems which are highlighted. To demonstrate the impact of roof slope on the distribution of stresses and the predicted strength, several purlin sections are evaluated for slopes varying from 0:12 to 4:12. For multi-span systems with very low slopes, the strength predicted by the proposed methodology is less than that predicted by the base test as a result of the higher loads and corresponding second order effects in the multi-span system. As the roof slope increases, stress distributions shift more towards the constrained bending distribution and show an increase in strength. At very steep slopes (4:12 or greater), as the roof system begins to deflect downslope, stress distributions change causing a rapid decrease in predicted strength. In this case, maximum stresses occur in the tension flange and it is expected that the purlin possesses substantial inelastic reserve capacity. It should also be noted that the predicted failure mechanism may change as the stress distributions change with increasing slope. For the investigated examples, while predicting the strength from base tests is conservative, the base test is not exactly representative of the behavior of the sloped roof.

Diaphragm stiffness in analysis is calibrated such that the measured lateral deflection in the base test matches the lateral displacement in the prediction methodology. To match the deflection in analysis, a stiffness that is much less than is derived from the cantilever test method must be used. As demand on the diaphragm increases, the stiffness must be reduced, indicating that to replicate the true behavior of the diaphragm it must be analyzed as non-linear. More work is required to better understand this behavior. It is a conservative approximation to use the linear stiffness calibrated to base tests as this approximation overestimates the shear demand in the diaphragm.

The analysis procedure does not explicitly calculate the global buckling strength of the system of purlins. In reasonably configured systems (torsion braces nominally near the third points), the braces prevent substantial rotation of the purlin, preventing a lateral torsional buckling mode from developing. As the proposed methodology incorporates first and approximated second order biaxial bending and torsion stresses, it essentially captures the local buckling interacting with the global buckling mode. Tests of such systems typically fail either by local or distortional buckling as a result of the combined restraint between the braces and the sheathing. Additional work is required to obtain the true global buckling strength. In lieu of a more detailed buckling analysis, it is recommended that the torsion braces have a stiffness that limits the rotation of the purlin at the brace location to 1/20.

References

AISI (American Iron and Steel Institute) (2016) *North American Specification for the Design of Cold-Formed Steel Structural Members*. AISI. Washington, DC. 2016.

AISI (American Iron and Steel Institute) (2017a) S901-17 *Rotational-Lateral Stiffness Test Method for Beam-to-Panel Assemblies*. AISI. Washington, DC. 2017.

AISI (American Iron and Steel Institute) (2017b) S907-17 *Test Standard for Determining the Strength and Stiffness of Cold-Formed Steel Diaphragms using the Cantilever Test Method*. AISI. Washington, DC. 2017.

AISI (American Iron and Steel Institute) (2017c). S908-17 *Base Test Method for Purlins Supporting a Standing Seam Roof System*. AISI. Washington, DC. 2017.

Emde, M. G. (2010) Investigation of Torsional Bracing of Cold-Formed Steel Roofing Systems. Master's Thesis. University of Oklahoma. Norman, OK. 2010.

Li, A., Schafer, B.W. (2010) "Buckling analysis of cold-formed steel members with general boundary conditions using CUFSM: conventional and constrained finite strip methods." *Proceedings of the 20th International Specialty Conference on Cold-Formed Steel Structures*. 2010.

Murray, T. M., Sears, J., and Seek, M. W. (2009). *D111-09 Design Guide for Cold-Formed Steel Purlin Roof Framing Systems*. AISI. Washington, DC.

Seaburg, P. A., Carter, C. J. (1997) *Steel Design Guide Series 9: Torsional Analysis of Structural Steel Members*. American Institute of Steel Construction. Chicago, IL. 1997.

Seek, M. W. and McLaughlin, D. (2017) "Impact of clip connection and insulation thickness on the bracing of purlins in standing seam roof systems." *Conference Proceedings, Structural Stability Research Council Annual Stability Conference*. 2017. Structural Stability Research Council, Chicago, IL.

Seek, M.W., Ramseyer, C. and Kaplan, I. (2016). "A Combined Direct Analysis and Direct Strength Approach to Predict the Flexural Strength of Z-Purlins with Paired Torsion Braces". *Proceedings of the 23rd International Specialty Conference on Cold-Formed Steel Structures*. 2016.

Seek, M.W., and Parva, A. (2018). "Predicting the Strength of Z-section purlins with One Flange Attached to Standing Seam Sheathing Using the Direct Strength Method". *Eighth International Conference on Thin-Walled Structures – ICTWS 2018*. Lisbon, Portugal, July 24-27, 2018.

Seek, M.W. (2018). "Flexural Strength of continuous-span Z-purlins with paired torsion braces using the Direct Strength Method". *Proceedings of the 24th International Specialty Conference on Cold-Formed Steel Structures*. 2018.

Zetlin, L and G. Winter. (1955). "Unsymmetrical Bending of Beams with and without Lateral Bracing." Journal of the Structural Division, ASCE, Vol. 81, 1955.

Appendix 1 – Summary of equations for sloped roof systems – simple span and multi-span interior bay

The following equations apply to simple span or multi-span interior sloped roof systems. The equations are based on the case where the system is nominally uniformly loaded, spacing and loading is nominally equal between adjacent purlins.

Uniform restraint force between purlin and sheathing

$$w_{rest} = w\left(\cos\theta\right)\rho \tag{A.1}$$

Where

$$\rho = \frac{C_1 \dfrac{\left(\dfrac{I_{xy}}{I_x}\right)L^4}{EI_{my}} + C_2 \dfrac{L^2 \tan\theta}{G'spa}}{C_1 \dfrac{L^4}{EI_{my}} + C_2 \dfrac{L^2}{G'spa}} \tag{A.2}$$

Simple span $$C_1 = \frac{1}{24}\cdot\left(\frac{c}{L}\right)\cdot\left[1-2\left(\frac{c}{L}\right)^2+\left(\frac{c}{L}\right)^3\right] \tag{A.3}$$

Multi-span interior $$C_1 = \frac{1}{24}\cdot\left(\frac{c}{L}\right)^2\cdot\left(1-\frac{c}{L}\right)^2 \tag{A.4}$$

Simple and multi-span $$C_2 = \frac{1}{2}\cdot\left(\frac{c}{L}\right)\cdot\left[1-\left(\frac{c}{L}\right)\right] \tag{A.5}$$

where

G′	= stiffness of diaphragm, lb/in.
L	= purlin span
spa	= purlin spacing (tributary panel width)
I_{my}	= modified moment of inertia = $\dfrac{I_x I_y - I_{xy}^2}{I_x}$
c	= distance from support location to brace location (see Figure 1)

Approximate mid-span lateral deflection

$$\Delta_{mid} = w\left(\rho\cos\theta - \sin\theta\right)\frac{L^2}{8G'\left(spa\right)} \tag{A.6}$$

Torsion

First order uniformly distributed torsion

$$t_{1st} = \left(w\cdot\cos\theta\right)\left(\rho\cdot e_{sy} - e_{sx}\right) \tag{A.7}$$

Second order parabolic torsion distribution

$$t_{2nd} = -\left(w \cdot \cos\theta\right)\Delta_{mid} \tag{A.8}$$

Brace torque from first order uniform torsion

$$T_{1st} = -C_3 t_{1st} L \tag{A.9}$$

$$\text{simple span} \quad C_3 = \frac{1}{4} \cdot \frac{1 - 2\left(\frac{c}{L}\right)^2 + \left(\frac{c}{L}\right)^3}{3\left(\frac{c}{L}\right) - 4\left(\frac{c}{L}\right)^2} \tag{A.10}$$

$$\text{multi-span} \quad C_3 = \frac{1}{4} \cdot \frac{\left(1 - \frac{c}{L}\right)^2}{\left(\frac{c}{L}\right)\left(2 - 3\frac{c}{L}\right)} \tag{A.11}$$

Brace torque from second order parabolic torsion

$$T_{2nd} = -C_4 t_{2nd} L \tag{A.12}$$

where

$$\text{simple span} \quad C_4 = \frac{1}{15} \cdot \frac{3 - 5\left(\frac{c}{L}\right)^2 + 3\left(\frac{c}{L}\right)^4 - \left(\frac{c}{L}\right)^5}{3\left(\frac{c}{L}\right) - 4\left(\frac{c}{L}\right)^2} \tag{A.13}$$

$$\text{multi-span} \quad C_4 = \frac{1}{15} \cdot \frac{3 - 5\left(\frac{c}{L}\right) + 3\left(\frac{c}{L}\right)^3 - \left(\frac{c}{L}\right)^4}{2\left(\frac{c}{L}\right) - 3\left(\frac{c}{L}\right)^2} \tag{A.14}$$

Net Brace Torque

$$T = T_{1st} + T_{2nd}$$

Brace equilibrium effects

Shear force in Torsion Brace

$$V = -\frac{2\left(T_{1st} + T_{2nd}\right)\xi}{spa} \tag{A.15}$$

Downslope purlin $\xi = 1$
Upslope purlin $\xi = -1$

Axial Force in brace (sign convention for force as applied to purlin)

$$P_b = -V\frac{I_{xy}}{I_x} \tag{A.16}$$

Moment about x-axis

The moment about the x-axis from the uniformly distributed loads at any location, z, along the span is

$$M_{x,dist} = w\cos(\theta)C_5 \tag{A.17}$$

$$\text{Simple span} \quad C_5 = \left(\frac{L^2}{2}\right)\left(\frac{z}{L}\right)\left(1-\frac{z}{L}\right) \tag{A.18}$$

$$\text{Multi-span} \quad C_5 = \frac{L^2}{12}\left(6\left(\frac{z}{L}\right)\left(1-\frac{z}{L}\right)-1\right) \tag{A.19}$$

The moment about the x-axis resulting from the shear force in the brace is

$$M_{x,V} = (V)C_6 \tag{A.20}$$

When $z \le c$

$$\text{Simple Span} \quad C_6 = z \tag{A.21}$$

$$\text{Multi-span} \quad C_6 = L\left(\frac{z}{L}-\frac{c}{L}\left(1-\frac{c}{L}\right)\right) \tag{A.22}$$

When $z \ge c$

$$\text{Simple Span} \quad C_6 = c \tag{A.23}$$

$$\text{Multi-span} \quad C_6 = \frac{c^2}{L} \tag{A.24}$$

The total moment about the x-axis is the sum of the two moment effects

$$M_x = M_{x,dist} + M_{x,V} \tag{A.25}$$

Distribution of bending stresses

The distribution of bending stresses across the cross section is calculated by

$$f_b = M_{x,dist}\left[\frac{-y}{I_{mx}} + \frac{x\frac{I_{xy}}{I_x}}{I_{my}} - \frac{x\cdot\rho}{I_{my}} + \frac{y\frac{I_{xy}}{I_y}\rho}{I_{mx}}\right] + M_{x,V}\left(\frac{-y}{I_x}\right) \tag{A.26}$$

Torsion stresses

Warping torsion normal stresses, f_w are calculated as presented in the AISC Torsion Analysis Design Guide (Seaburg and Carter, 1997) considering both pure torsion and warping torsion resistance.

$$f_w = E\cdot W_N\cdot\left(\phi_u\text{ "}+\phi_p\text{ "}+\phi_{brace}\text{ "}\right) \tag{A.27}$$

The generalized warping functions are given for each of the torsional load effects: uniform torsion, parabolic distributed torsion, and concentrated torque at the brace location

Uniform torsion

Simple span

Any location, z $$\phi_u'' = \frac{t_{1st}}{GJ}\left(\cosh\left(\frac{z}{a}\right) - \tanh\left(\frac{L}{2a}\right)\sinh\left(\frac{z}{a}\right) - 1\right) \quad \text{(A.28)}$$

Mid-span $$\phi_u'' = \frac{t_{1st}}{GJ}\left(\frac{1}{\cosh\left(\frac{L}{2a}\right)} - 1\right) \quad \text{(A.29)}$$

Brace $$\phi_u'' = \frac{t_{1st}}{GJ}\left(\cosh\left(\frac{c}{a}\right) - \tanh\left(\frac{L}{2a}\right)\sinh\left(\frac{c}{a}\right) - 1\right) \quad \text{(A.30)}$$

Multi-span

Any location, z $$\phi_u'' = \frac{t_{1st}}{GJ}\left(\left(\frac{L}{2a}\right)\left(\frac{\cosh\left(\frac{L}{2a}\right)}{\sinh\left(\frac{L}{2a}\right)}\right)\cosh\left(\frac{z}{a}\right) - \left(\frac{L}{2a}\right)\sinh\left(\frac{z}{a}\right) - 1\right) \quad \text{(A.31)}$$

Mid-span $$\phi_u'' = \frac{t_{1st}}{GJ}\left(\left(\frac{L}{2a}\right)\frac{1}{\sinh\left(\frac{L}{a}\right)} - 1\right) \quad \text{(A.32)}$$

Brace $$\phi_u'' = \frac{t_{1st}}{GJ}\left(\left(\frac{L}{2a}\right)\left(\frac{\cosh\left(\frac{L}{2a}\right)}{\sinh\left(\frac{L}{2a}\right)}\right)\cosh\left(\frac{c}{a}\right) - \left(\frac{L}{2a}\right)\sinh\left(\frac{c}{a}\right) - 1\right) \quad \text{(A.33)}$$

Parabolic torsion

Simple span

Any location, z $$\phi_p'' = \frac{t_{2nd}}{GJ}\left[\frac{8a^2}{L^2}\left(1 - \cosh\left(\frac{z}{a}\right) + \frac{\cosh\left(\frac{L}{a}\right) - 1}{\sinh\left(\frac{L}{a}\right)}\sinh\left(\frac{z}{a}\right)\right) + 4\left(\frac{z}{L}\right)^2 - 4\left(\frac{z}{L}\right)\right] \quad \text{(A.34)}$$

Mid-span $$\phi_p'' = \frac{t_{2nd}}{GJ}\left[\frac{8a^2}{L^2}\left(1 - \frac{1}{\cosh\left(\frac{L}{2a}\right)}\right) - 1\right] \quad \text{(A.35)}$$

Brace Location $\phi_p'' = \frac{t_{2nd}}{GJ}\left[\frac{8a^2}{L^2}\left(\frac{\cosh\left(\frac{L}{a}\right)-1}{\sinh\left(\frac{L}{a}\right)}\sinh\left(\frac{c}{a}\right)-\cosh\left(\frac{c}{a}\right)+1\right)+4\left(\frac{c}{L}\right)^2-4\left(\frac{c}{L}\right)\right]$ (A.36)

Multi-span

Any location, z $\phi_p'' = \frac{t_{2nd}}{GJ}\left[\frac{L}{a}\left(\frac{1}{3}-\frac{4a^2}{L^2}\right)\left(\frac{\cosh\left(\frac{L}{2a}\right)}{\sinh\left(\frac{L}{2a}\right)}\cosh\left(\frac{z}{a}\right)-\sinh\left(\frac{z}{a}\right)+1\right)+4\left(\frac{z}{L}\right)^2-4\left(\frac{z}{L}\right)+\frac{8a^2}{L^2}\right]$ (A.37)

Mid-span $\phi_p'' = \frac{t_{2nd}}{GJ}\left[\frac{L}{a}\left(\frac{1}{3}-\frac{4a^2}{L^2}\right)\left(\frac{1}{\sinh\left(\frac{L}{2a}\right)}\right)+\frac{8a^2}{L^2}-1\right]$ (A.38)

At brace location $\phi_p'' = \frac{t_{2nd}}{GJ}\left[\frac{L}{a}\left(\frac{1}{3}-\frac{4a^2}{L^2}\right)\left(\frac{\cosh\left(\frac{L}{2a}\right)}{\sinh\left(\frac{L}{2a}\right)}\cosh\left(\frac{c}{a}\right)-\sinh\left(\frac{c}{a}\right)+1\right)+4\left(\frac{c}{L}\right)^2-4\left(\frac{c}{L}\right)+\frac{8a^2}{L^2}\right]$ (A.39)

Concentrated brace torque

Simple span

z < c $\phi_{brace}'' = \frac{T_{1st}+T_{2nd}}{GJ}\left(\frac{1}{a}\right)\sinh\left(\frac{z}{a}\right)\left(\frac{\sinh\left(\frac{c}{a}\right)+\sinh\left(\frac{L-c}{a}\right)}{\tanh\left(\frac{L}{a}\right)}-\cosh\left(\frac{c}{a}\right)-\cosh\left(\frac{L-c}{a}\right)\right)$ (A.40)

c < z < (L-c) $\phi_{brace}'' = \frac{T_{1st}+T_{2nd}}{GJ}\left(\frac{1}{a}\right)\left[\sinh\left(\frac{z}{a}\right)\left(\frac{\sinh\left(\frac{c}{a}\right)+\sinh\left(\frac{L-c}{a}\right)}{\tanh\left(\frac{L}{a}\right)}-\cosh\left(\frac{L-c}{a}\right)\right)-\cosh\left(\frac{z}{a}\right)\sinh\left(\frac{c}{a}\right)\right]$ (A.41)

At mid-span $\phi_{brace}'' = \frac{T_{1st}+T_{2nd}}{GJ}\left(\frac{1}{a}\right)\left[\sinh\left(\frac{L}{2a}\right)\left(\frac{\sinh\left(\frac{c}{a}\right)+\sinh\left(\frac{L-c}{a}\right)}{\tanh\left(\frac{L}{a}\right)}-\cosh\left(\frac{L-c}{a}\right)\right)-\cosh\left(\frac{L}{2a}\right)\sinh\left(\frac{c}{a}\right)\right]$ (A.42)

At brace location $\phi_{brace}'' = \frac{T_{1st}+T_{2nd}}{GJ}\left(\frac{1}{a}\right)\sinh\left(\frac{c}{a}\right)\left(\frac{\sinh\left(\frac{c}{a}\right)+\sinh\left(\frac{L-c}{a}\right)}{\tanh\left(\frac{L}{a}\right)}-\cosh\left(\frac{c}{a}\right)-\cosh\left(\frac{L-c}{a}\right)\right)$ (A.43)

Multi-span

z < c $\phi_{brace}'' = \frac{T_{1st}+T_{2nd}}{GJ}\left(\frac{1}{a}\right)\left(\left(\frac{\cosh\left(\frac{L}{2a}\right)}{\sinh\left(\frac{L}{2a}\right)}\left(1-\cosh\left(\frac{c}{a}\right)\right)+\sin h\left(\frac{c}{a}\right)\right)\cosh\left(\frac{z}{a}\right)-\sinh\left(\frac{z}{a}\right)\right)$ (A.44)

c < z < (L-c)
$$\phi_{brace}'' = \frac{T_{1st} + T_{2nd}}{GJ}\left(\frac{1}{a}\right)\left(1-\cosh\left(\frac{c}{a}\right)\right)\left(\frac{\cosh\left(\frac{L}{2a}\right)}{\sinh\left(\frac{L}{2a}\right)}\cosh\left(\frac{z}{a}\right)-\sinh\left(\frac{z}{a}\right)\right) \quad (A.45)$$

At mid-span
$$\phi_{brace}'' = \frac{T_{1st} + T_{2nd}}{GJ}\left(\frac{1}{a}\right)\left[\left(1-\cosh\left(\frac{c}{a}\right)\right)\left(\frac{1}{\sinh\left(\frac{L}{2a}\right)}\right)\right] \quad (A.46)$$

At brace location
$$\phi_{brace}'' = \frac{T_{1st} + T_{2nd}}{GJ}\left(\frac{1}{a}\right)\left(1-\cosh\left(\frac{c}{a}\right)\right)\left(\frac{\cosh\left(\frac{L}{2a}\right)}{\sinh\left(\frac{L}{2a}\right)}\cosh\left(\frac{c}{a}\right)-\sinh\left(\frac{c}{a}\right)\right) \quad (A.46)$$

Summation of stresses

The net stress, f, at each location in the cross section is the sum of the bending and torsion warping stresses.

$$f = f_b + f_w \quad (A.47)$$

Strength evaluation

The net stress is calculated at each point of interest along the span of the purlin. Typically, the critical locations to check the strength are the mid-span of the purlin and the brace locations.

Scaling stresses

The maximum stress, f_{max}, in the cross section is determined. The stress scale factor is determined from the ratio of the yield stress of the material to the peak stress in the cross section, F_y/f_{max}. The stress at each location of the cross section is multiplied by the stress scale factor to scale the stresses in the cross section to the point of first yield.

Buckling analysis

A finite strip buckling analysis is performed in CUFSM using the cross section stresses scaled to the point of first yield. In the analysis, no lateral or rotational springs are applied because the both the local and distortional buckling half sine wavelength is shorter than the typical spacing between standing seam clip attachments. From the minima in signature curve in CUFSM, buckling load factors are determined for local and distortional buckling.

Strength determination

At the location along the span being evaluated, the yield moment, M_y, is calculated from the product of the moment about the x-axis, M_x, and the stress scale factor.

$$M_y = M_x\left(\frac{F_y}{f_{max}}\right) \quad (A.48)$$

Local buckling

The critical local buckling moment, $M_{cr\ell}$, is calculated as the product of the local buckling load factor from CUFSM and the yield moment. The nominal local buckling strength, $M_{n\ell}$ is

calculated according to AISI S100 Section F3.2 with $F_n = F_y$.

Distortional buckling

The critical distortional buckling moment, $M_{crd,}$ is calculated as the product of the distortional buckling load factor from CUFSM and the yield moment. The nominal distortional buckling strength is calculated according to AISI S100 Section F4.1.

Controlling strength

The minimum of the local and distortional buckling moment is the nominal strength, M_n. which is then compared to the moment about the x-axis, M_x. If $M_n > M_x$, the purlin has sufficient capacity to support the uniform load. The calculated nominal strength in this case does not necessarily represent the actual strength. Because the process includes an approximation of second order effects, the stress distribution will change at different load levels. If the actual failure load is required, iteration is required by varying the applied load until M_n is approximately equal to M_x. Iteration may be terminated when M_n is within ten percent of M_x.

Calculate the ratio of M_n/M_x at each of the critical locations along the length of the purlin. The location where the ratio of M_n/M_x is the largest is the location that will control the strength.

American Iron and Steel Institute

25 Massachusetts Avenue, NW
Suite 800
Washington, DC 20001

www.steel.org

Research Report RP-19-3